The Evolution of Barred Disks as a Function of Environment: Constraints from the Abell 901/2 Supercluster with STAGES

Irina Marinova[1], Shardha Jogee[1], Amanda Heiderman[1], David Bacon[9], Michael Balogh[10], Marco Barden[11], Fabio D. Barazza[4], Eric F. Bell[6], Asmus Böhm[12], John A.R. Caldwell[18], Meghan E. Gray[3], Boris Häußler[3], Catherine Heymans[2,5], Knud Jahnke[6], Eelco van Kampen[11], Sergey Koposov[6], Kyle Lane[3], Daniel H. McIntosh[15], Klaus Meisenheimer[6], Chien Y. Peng[7,8], Hans-Walter Rix[6], Sebastian F. Sánchez[13], Rachel Somerville[6], Andy Taylor[14], Lutz Wisotzki[12], Christian Wolf[16], & Xianzhong Zheng[17]

marinova@astro.as.utexas.edu, sj@astro.as.utexas.edu, alh@astro.as.utexas.edu

[1]Department of Astronomy, University of Texas at Austin, Austin, TX

[2]Department of Physics and Astronomy, University of British Columbia, Vancouver, Canada

[3]School of Physics and Astronomy, The University of Nottingham, Nottingham, UK

[4]Laboratoire d'Astrophysique, École Polytechnique Fédéralede Lausanne, Observatoire, Sauverny, Switzerland

[5]Institut d'Astrophysique de Paris, Paris, France

[6]Max-Planck-Institut für Astronomie, Königstuhl 17, Heidelberg, Germany

[7]NRC Herzberg Institute of Astrophysics, Victoria,Canada

[8]Space Telescope Science Institute, Baltimore, MD, USA

[9]Institute of Cosmology and Gravitation, University of Portsmouth, Portsmouth, UK

[10]Department of Physics and Astronomy, University Of Waterloo, Ontario, Canada

[11]Institute for Astro- and Particle Physics, University of Innsbruck, Innsbruck, Austria

[12]Astrophysikalisches Insitut Potsdam, Potsdam, Germany

[13]Centro Hispano Aleman de Calar Alto, Almeria, Spain

[14]The Scottish Universities Physics Alliance, Institute for Astronomy, University of Edinburgh, Edinburgh, UK

[15]Department of Astronomy, University of Massachusetts, Amherst, MA, USA

[16]Department of Astrophysics, University of Oxford, Oxford, UK

[17]Purple Mountain Observatory, National Astronomical Observatories, Chinese Academy of Sciences, Nanjing, China

[18]University of Texas, McDonald Observatory, Fort Davis, TX, USA

ABSTRACT

We present a study of ~ 800 bright ($M_{\rm V} \leq$ -18), intermediate mass ($M/M_{\odot} \sim 10^9$) galaxies in the Abell 901/2 supercluster at z ~ 0.165. Multi-wavelength coverage is available from the Space Telescope Abell 901/2 Galaxy Evolution Survey (STAGES) and COMBO-17 surveys. This STAGES survey provides a unique opportunity to study how the evolution of bars and their host disks is affected by a dense cluster environment. We identify and characterize bars through ellipse-fitting. A complementary visual classification scheme is used to characterize other morphological features (e.g., bars, spiral arms, rings, bulge-to-disk ratio, and clumpiness). We find the following results. (1) The bar fraction is traditionally defined as the number of barred disks over the total number of disk galaxies, $f_{\rm bar} = N_{\rm barred}/N_{\rm disk}$, so we explore the issues of disk selection in a cluster environment. Using a color cut to select disks would miss 24% – 54% of disk galaxies on the red sequence and a Sérsic cut ($n \leq 2.5$) would miss 24% – 37% of disk galaxies, when compared to visually classified disks. Therefore, a blind application of these disk selection methods would miss many red, bulge-dominated disk galaxies, which are prevalent in a cluster environment. (2) However, the optical bar fraction remains similar within 3%, irrespective of which method is used for disk selection. $F_{\rm bar} = 32\% \pm 6\%$, $29\% \pm 6\%$, and $28\% \pm 6\%$, respectively, for the three methods of disk selection (visual, color, and Sérsic), with the bar being characterized by ellipse fitting. (3) The bar fraction is approximately twice as high in galaxies with the lowest central concentration ($f_{\rm bar} \sim 46\% \pm 9\%$) compared to galaxies with the highest central concentration ($f_{\rm bar} \sim 17\% \pm 4\%$). The bar fraction is ~ 1.6 times higher in galaxies visually classified as 'clumpy/dusty' ($f_{\rm bar} \sim 44\% \pm 5\%$) compared to galaxies classified as 'smooth' ($f_{\rm bar} \sim 27\% \pm 3\%$). (4) We trace local environment density using projected mass density κ, Σ_{10}, ICM density from X-ray emission, and the projected distance to the nearest cluster center. We find no significant trend of the fraction of disk galaxies that are barred with any of the four tracers of environment density. The fraction of visually identified 'clumpy/dusty' disk galaxies decreases with density, and we recover the well-known morphology-density relation. (4) The optical bar fraction in the cluster, $f_{\rm bar,STAGES} \sim 30 \pm 6\%$ is comparable to the optical bar fraction found for field galaxies (e.g., $f_{\rm bar,FIELD} \sim 44\% \pm 6\%$) within the range of uncertainty. Taken together, our results suggest that the processes that affect bar formation and destruction are overwhelmingly dictated by particular properties of the host galaxy, and not the local environment in which the galaxy currently lives. In particular, our results suggest that it is easier to form and/or sustain a bar in

galaxies with low central concentration and high gas content.

1. Introduction

It has been well established that the evolution of galaxies is affected by their environment. In one scenario of cold dark matter (CDM) cluster formation, the observed morphology-density dependence of galaxies (e.g., Oemler 1974; Dressler 1980) can be accounted for by the initial conditions dictating the primordial density fluctuations from which cluster galaxies condensed (Evrard 1990). In other words, clusters show a different galaxy population from the field because galaxies form earlier in overdense regions and are thus older than galaxies in the field. Alternatively, clusters grow through accretion of field galaxies or groups of galaxies (Zabludoff & Franx 1993; Abraham et al. 1996; Balogh et al. 2000; Kodama et al. 2001; Treu et al. 2003; Wolf, Gray, & Meisenheimer 2005). During this process spirals are transformed into spheroid-dominated galaxies such as ellipticals and S0's through a variety of mechanisms, unique to a dense cluster environment. Specifically, galaxies can undergo multiple, frequent interactions with other galaxies ('galaxy harassment'; Moore et al. 1996; 1998) and the cluster tidal field (Byrd & Valtonen 1990; Bekki 1999). Ram-pressure stripping can deprive spirals of their cold gas (e.g., Gunn & Gott 1972) while their hot, diffuse gas envelopes are stripped away through 'strangulation' (Larson, Tinsley, & Caldwell 1980). All of these effects can combine to drive galaxy evolution, making the galaxy population in present-day clusters noticeably different than that of clusters at intermediate redshifts (Butcher-Oemler effect; e.g., Butcher & Oemler 1978).

But what is the relationship between these environmental effects and internal drivers of galaxy evolution such as stellar bars? For field galaxies in the local universe, bars are known to be the most efficient way to redistribute material in the galaxy disk (Combes & Sanders 1981; Weinberg 1985; Debattista & Sellwood 1998, 2000; Athanassoula 2002). Bars channel gas into the central regions of galaxies, where powerful starbursts can ignite (Schwarz 1981; Shlosman, Frank, & Begelman 1989; Teuben 1996; Kormendy & Kennicutt 2004; Jogee, Scoville, & Kenney 2005; Sheth et al. 2005), building central disky structures known as 'pseudobulges' (Kormendy 1982; Kormendy 1993; Fisher 2006).

The detailed process of bar formation is not yet known, but simulations suggest that a cold disk, with low velocity dispersion, σ, favors the formation of spontaneous disk instabilities. External triggers, such as tidal interactions can also induce bars in a dynamically cold disk (e.g., Hernquist & Mihos 1995). Thus, the cluster processes described above can have competing effects on bar formation. Frequent tidal interactions can induce stellar bars, however they may also heat the disks and make them less susceptible to bar formation. Dubinski

et al. (2008) explored these effects by modeling the interaction of a hundred DM satellites on M31. They found that while the satellites did not have a large heating effect on the disk, encounters close to the galaxy center could produce strong non-axisymmetric instabilities such as stellar bars (Dubinski et al. 2008). However, in dense clusters, disk galaxies that are deprived of their cold gas through ram-pressure stripping may be too dynamically hot to form bars. In the scenario whereby clusters grow by accretion of field galaxies, these processes may have no effect on an already existing bar. Therefore, the fraction of barred galaxies in a cluster depends on the interplay between these effects, on the epoch of bar formation, and on the evolutionary history of clusters.

There have been only a handful of observational studies that have explored impact of environment on barred disks. Using a uniform sample of 930 galaxies from the Shapley-Ames catalog, where bar classifications were performed through visual inspection of optical images, van den Bergh (2002) found no difference between the bar fraction in the field and in clusters, and therefore concluded that the bar fraction depends solely on host-galaxy properties. It should be noted that for this study, the environment assignments were largely qualitative, made by inspecting the region around the galaxy on the image, and looking at luminosities and radial velocities of surrounding galaxies. Varela et al. (2004) found that the bar fraction is almost twice as high in galaxies that are interacting, compared to isolated galaxies. This study relied on redshifts from the CfA survey to determine whether a galaxy was being perturbed by a close companion, however their morphological bar classifications came from LEDA and NED which have been known to be notoriously inhomogeneous. Recently, Mendez-Abreu, Aguerri, & Corsini (2008) studied the effects of environment on barred galaxies using ~ 3000 galaxies from SDSS-DR5, and found that the bar fraction and properties were not correlated to galaxy environment. However, they excluded interacting galaxies from their study.

We are now in a position to make further progress in this largely unexplored aspect of galaxy evolution with the STAGES panchromatic dataset, which includes: a 5×5 square degree HST ACS mosaic of the A901/2 supercluster, spectrophotometric redshifts from COMBO-17, coverage with XMM-Newton, GALEX, and *Spitzer*, as well as dark matter maps. We explore the frequency of bars as a function of host galaxy stellar mass, and as a function of cluster radius, galaxy number density, ICM density, and DM density. It should be noted that traditionally the bar fraction $f_{\rm bar}$ is defined as the fraction of *disk galaxies* that are barred. Hence calculation of $f_{\rm bar}$ requires disk galaxies to be reliably identified. In this paper, we draw attention to the fact that many automated methods commonly used to identify disks in the field may fail in clusters. Motivated by this, we explore different ways of identifying disks (e.g., color cut, Sérsic cut, visual classification) and explore the effect on $f_{\rm bar}$.

2. Data and Sample Selection

The Abell 901/902 supercluster consists of three galaxy clusters and a group at z$\sim$ 0.165, with an average separation of 1 Mpc. The properties of this system are described in detail in Gray et al. (2002). The STAGES survey (Gray et al. 2008) covers a 5 $\times$ 5 square degree field centered on the supercluster, consisting of an 80 tile mosaic with the HST ACS F606W. The ACS point spread function (PSF) of 0.1″ corresponds to $\sim$ 282 pc at z $\sim$ 0.165[19]. Spectro-photometric redshifts are available for all galaxies from COMBO-17 (Wolf et al. 2004; 2005) with δz/(1+z) $\sim$ 0.02 down to R_{Vega} = 24. The multi-wavelength dataset includes X-ray maps of the ICM density from XMM-Newton, UV from GALEX, *Spitzer* 24μ coverage, and dark matter maps from weak lensing (Gray et al. 2002; Heymans et al. 2008). Total star formation rates (SFRs) derived from UV and *Spitzer* 24μ, as well as stellar masses (Borch et al. 2006) are also available for this field.

Cluster galaxies are selected using the photometric redshifts. This provides a cluster sample of 2136 galaxies with a 90% confidence down to R_{Vega}= 24. For this paper, we focus on galaxies brighter than $M_V \leq -18$. We choose this cutoff, because it tends to separate well the regimes where normal and dwarf galaxies dominate on the luminosity functions of clusters (Binggeli, Sandage, & Tammann 1988). We do not consider dwarf galaxies in this study for two reasons. First, our resolution of $\sim$ 282 pc may be insufficient in many cases to reliably identify morphological structures such as bars in smaller dwarf galaxies. Second, the contamination of the sample by field galaxies fainter than $M_V > -18$ becomes significant. This leaves us with a sample of 795 bright ($M_V \leq -18$), cluster galaxies.

3. Methodology

3.1. Characterization of Bars

We use the standard IRAF task 'ellipse' to fit ellipses to the galaxy isophotes out to a_{max}, where a_{max} is the radius at which the surface brightness reaches sky level. This method of ellipse fitting has been widely used to identify and characterize bars (e.g., Wozniak et al. 1995; Friedli et al. 1996; Regan et al. 1997; Mulchaey & Regan 1997; Jogee et al. 1999, 2002a, 2002b, 2004; Knapen et al. 2000; Laine et al. 2002; Sheth et al. 2003; Elmegreen et al. 2004; Marinova & Jogee et al. 2007; Menéndez-Delmestre et al. 2007). We employ an iterative wrapper, developed by Jogee et al. (2004), which runs the task 'ellipse' up to 100

[19]We assume in this paper a flat cosmology with $\Omega_M = 1 - \Omega_\Lambda = 0.3$ and H_0 =70 km s^{-1} Mpc^{-1}.

times for each galaxy, until an ellipse is able to be fitted at every radial increment out to $a_{\rm max}$. Characterizing the goodness of the ellipse fits is described in more detail in Marinova & Jogee (2007; hereafter MJ07). We were able to successfully fit 772/795 (97%) of galaxies in our bright cluster sample.

We overlay the fitted ellipses onto the galaxy images and plot the radial profiles of surface brightness (SB), ellipticity (e), and position angle (PA). We use both the overlays and radial profiles to classify the galaxies as 'inclined', 'unbarred', or 'barred'. Galaxies classified as 'inclined' have an outermost isophote with $e > 0.5$, corresponding to $i > 60°$. Because it is difficult to identify morphological structures in such highly inclined galaxies, we do not attempt to classify them as 'barred' or 'unbarred'. For galaxies with moderate inclinations (i$< 60°$), we classify a galaxy as barred if: (1) the e rises smoothly to a global maximum, $e_{\rm bar} > 0.25$, while the PA remains relatively constant (within $\sim$ 20°) and (2) the e then drops by at least 0.1 and the PA changes at the transition between the bar and disk region. After discarding highly inclined galaxies (232 or 30%) and those with visually-identified poor fits (53 or 7%), we are left with 487 moderately inclined (i$< 60°$), bright ($M_V \leq -18$) cluster galaxies.

The luminosity and color distributions of the total fitted sample of 772 bright, cluster galaxies and the moderately inclined sample of 487 galaxies are overplotted in Figure 1(a) and (b), respectively. An example of the overalys and radial profiles of a barred cluster galaxy are shown in Figure 2. Because we are looking at optical wavelengths, in rare cases the criterion of constant PA in the bar region may not be satisfied. This can happen in galaxies where the bar is weak, and the dust lanes along the leading edges of the bar are curved, producing a 'twisting' in the PA radial profile (Athanassoula 1992b). We find 38 such cases (6%), which we classify as 'unbarred' because they do not satisfy the constant PA criterion. The advantages and limitations of the ellipse-fitting method are further discussed in detail in MJ07.

In addition to quantitatively identifying and characterizing bars using ellipse fitting, we also visually classify all galaxies in the sample. The identification of bars through visual inspection provides an independent check for the detection of bars through ellipse-fits.

3.2. Issues on Disk Selection

In all studies conducted to date, the bar fraction, $f_{\rm bar}$ has been defined as the number of barred *disk* galaxies divided by the total number of *disk* galaxies:

$$f_{\rm bar} = \frac{N_{\rm bar}}{N_{\rm disk}}. \quad (1)$$

In this paper we use the term 'disk galaxies' to describe all galaxies with a disk component (e.g., S0-Sm). The bar fraction is only quoted with disk galaxies in mind, because bars are believed to be an $m = 2$ instability in the disk component of galaxies. In the local universe, for nearby galaxies, catalogs like the RC3 (deVaucouleurs et al. 1991) contain reliable classifications of galaxy morphology, making it possible to select a sample of only disk galaxies for bar studies. In large surveys such as the SDSS and GEMS, two quantitative methods have been used to pick out disk galaxies: (1) using a color cut in color-magnitude space and (2) using a Sérsic index cut to select disks. In the color cut method, only blue cloud galaxies are selected on a color-magnitude diagram (Bell et al. 2004; Barden et al. 2004; Jogee et al. 2004; Ravindranath et al. 2004; Barazza, Jogee, & Marinova 2008; hereafter BJM08). The Sérsic cut method involves selecting only galaxies with Sérsic index n$<$ 2.5. This is motivated by the fact that a pure disk should have a Sérsic index of 1, while an elliptical galaxy should have a Sérsic index of 4. Simulations have shown that the value n = 2.5 is a good dividing line in separating disks from spheroidals.

Using a color or Sérsic cut to pick out disk galaxies works fairly well in the field. However, these methods can fail in a cluster environment, where the galaxy populations are different than those in the field. Gas stripping of spirals could quench their star formation and make them look redder. These galaxies might then be missed by a color cut. On the other hand, the prevalence of bulge-dominated S0-type disk galaxies in clusters (Dressler 1980) could be missed by a Sérsic cut. For this reason, we use a third method to pick out disk galaxies: visual classification (see § 4.1).

We visually classify the whole sample and put galaxies into different groups according to the galaxy morphology and a rough visual estimation of the bulge to disk ratio. A galaxy is identified as a disk galaxy if it exhibits the dynamical signatures of disk instabilities such as a stellar bars and spiral arms. In the absence of such structure, disks are picked by an identifiable break between the bulge and disk component either in the image itself and/or using an estimation of the brightness profile with ds9. Disk galaxies are further subdivided into two classes according to bulge-to-disk ratio: 'bulge+disk' and 'pure disk'. Pure disk galaxies are those where no central spheroidal component is seen. Conversely, a galaxy is classified as a pure bulge if its morphology is spheroidal and there is no break in the brightness profile, indicative of the transition between the bulge-dominated and disk-dominated region. In addition, pure bulge galaxies do not exhibit disk features such as spiral arms or stellar bars. Figure 3 shows examples of the morphological visual classes. Panel (a) shows a galaxy classified as 'pure bulge'. Panels (b) – (e) show examples of 'bulge+disk' galaxies, while panels (f) – (i) show examples of 'pure disk' galaxies.

The main strength of this visual classification scheme is that it broadly separates

elliptical-type galaxies from galaxies that have strong disk components independent of other factors such as color or gas and dust content (§ 3.3). Three classifiers (S.J., A.H., I.M.) completed a training set of several hundred galaxies, and two classifiers (A.H., I.M.) classified the full cluster sample. Subsequently, uncertain cases were reviewed by all three classifiers. It should be noted that there is inherent difficulty in differentiating between pure bulge and high bulge-to-disk ratio galaxies (e.g., S0) that do not exhibit spiral structure. The two classifiers (I.M. and A.H.) could not reach agreement on 4% of cases regarding whether a galaxy was a pure bulge or contained a disk component.

3.3. Presence of Gas and Dust in Galaxies

The gas and dust content of galaxies holds information about their formation history and dynamical state. In the traditional Hubble classification scheme, the gas/dust content increases with decreasing bulge-to-disk ratio toward late-type galaxies. Local field galaxies are well described by such a sequence. However, there is evidence that the Hubble classification scheme breaks down in dense clusters. Koopmann & Kenney (1998) show that the effects of the cluster processes described in § 1 are such that the central concentration of galaxies no longer correlates with their star formation activity, as it does in the field. This suggests that in clusters effects such as ram-pressure stripping or galaxy harassment can alter the gas content of galaxies. The result is that one can no longer assume a correlation between gas/dust content and bulge-to-disk ratio.

Particularly important for this study is the fact that a high amount of gas and dust makes it more difficult to identify a stellar bar at optical wavelengths. MJ07 show that, because of obscuration by gas and dust in the optical, the bar fraction is higher in the infrared (IR) H band by $\sim 15\%$ for galaxies at $z \sim 0$.

Motivated by these considerations, we attempt to visually characterize the gas/dust content of galaxies independently from their morphological class. The degree of 'clumpiness' in a galaxy is used as a rough proxy for classification of the amount of gas present. We allocate galaxies into two broad classes: (1) 'smooth'/mostly gas free or (2) 'clumpy'/mostly gas rich. Examples of 'smooth'/gas poor galaxies are shown in panels (a), (b), (c), (h), and (i) of Figure 3. 'Clumpy'/gas rich galaxies are shown in panels (d) – (g) of Figure 3.

4. Results and Discussion

4.1. Selection of Disk Galaxies in Clusters

How well do the Sérsic and color cut methods pick out disk galaxies when compared to visual classification? Figure 4 shows visually identified disk galaxies plotted in blue on a rest-frame color vs. M_V (panel a) and rest-frame color vs. Sérsic index (panel b) diagram. Selecting blue cloud galaxies only picks out 46%± 4% of galaxies selected as disks by visual classification, consistent with a high number of red disks in the cluster environment. This implies that 54%± 4% of the red sequence is made up of visually-selected disk galaxies. This is a surprisingly high value, and so we explore the nature of these red galaxies in more detail. One possibility for this result is that because of the unavoidable uncertainty between the classifications of 'pure bulge' (e.g., E's) and 'B+D smooth' (e.g., S0's), some of our 'B+D smooth' galaxies on the red sequence are really ellipticals. This is a plausible scenario, as 90% of the disk galaxies identified visually on the red sequence are 'B+D smooth' galaxies. However, the uncertainty between the two classes ('B+D smooth' vs. 'pure bulge') is present only when the 'B+D smooth' galaxy does not display unambiguous disk signatures such as spiral arms and stellar bars (plotted as large green points in Figure 4). Therefore, we can put a firm lower limit on the number of disk galaxies on the red sequence if we take as unambiguous disks only galaxies which are (1) clumpy (have a large amount of gas/dust) or (2) smooth galaxies that display an unambiguous dynamical disk signature such as a stellar bar or spiral arms. In this case, 24% (74/303) of the moderately-inclined galaxies on the red sequence exhibit such disk signatures.

Taking galaxies with Sérsic index $n < 2.5$ picks out 63%± 4% of galaxies visually selected as disks. The Sérsic cut method will pick up many of the red disks that the color cut misses, however the Sérsic cut method might miss some early-type disk galaxies with very prominent bulges or very clumpy galaxies with large star formation regions in their outer disks. In addition, the presence of an AGN will drive the Sérsic index to high values. Again, to put a firm lower limit on the number of disk galaxies that are missed by a Sérsic cut, we use criteria (1) and (2) above. This tells us that at least 24% (56/225) of the galaxies with $n > 2.5$ are disk galaxies.

4.2. Global Properties of Visual Classes

Figure 5(a,b,c) shows the absolute M_V magnitude, rest-frame $U - V$ color, and stellar mass properties of the different visual morphological classes, respectively. Galaxies classified as 'pure bulge' have an M_V distribution, spanning the whole range of absolute magnitudes,

all the way from -24 to -18. This is expected, because this class contains not only the largest giant ellipticals, but also some bright dwarf ellipticals, which have made the cut at the faint magnitude end close to $M_V \sim$ -18. Galaxies classified as 'B+D clumpy' have the highest average luminosity, peaking around $M_V \sim$ -20.5. The high average luminosity of this class makes sense in light of the fact that this class represents Sb-type spirals, which are massive and star-forming. As expected, the lowest-luminosity galaxies are represented by those classified as 'pure disks'. The class 'pure disk clumpy', with an average absolute magnitude of -19.3, represents the late end of the Hubble sequence (e.g., Sc-Sm). The class 'pure disk smooth' likely consists of some bright dwarf galaxies, or perhaps late-type spirals, which have been stripped of their gas due to cluster processes such as ram-pressure stripping.

The visual classes are very well separated in color space, as seen in panel (b) of Figure 5. As expected, the reddest galaxies are those classified as 'pure bulge' (e.g., ellipticals) and 'B+D smooth' (e.g., S0-Sa), peaking at U-V$\sim$ 1.4. These galaxies are expected to primarily consist of old stars, and not much gas and dust, hence giving them a smooth appearance and red rest-frame color. The bluest galaxies are the ones classified as 'pure disk clumpy' (U-V$\sim$ 0.4), which have blue colors presumably because of their high specific SFRs. Galaxies classified as 'B+D clumpy' occupy the middle of the color distribution, and are likely comprised of a mix of old and young stars with a significant amount of dust.

The stellar mass distribution shown in panel (c) of Figure 5, shows a separation between the galaxy classes with most ellipticals and giant spirals ('B+D clumpy', 'B+D smooth') on the high-mass end ($\log(M/M_\odot) \sim$ 10.5) and 'pure disk' late-type galaxies on the low-mass end ($\log(M/M_\odot) \sim$ 9.5).

4.3. Bar Fraction

For the STAGES cluster sample, three methods of selecting disks are available: visual classification, blue cloud selection, and Sérsic cut selection. Because of the problems in selecting disks in a cluster sample using the quantitative color or Sérsic cuts (see § 3.2 and 4.1), we estimate f_{bar} using visual classification to select disk galaxies. We obtain a bar fraction $f_{bar} = 32\% \pm 6\%$. Comparison of the bar fraction to the bar fraction found for field samples is discussed in § 4.6

For completeness, we also calculate the bar fraction using a color cut and Sérsic cut to select disk galaxies. The results are shown in Table 1 for bright ($M_V \leq -18$) galaxies, and in Table 2 for galaxies with $\log(M/M_\odot) > 9$. In all cases, regardless of the disk selection method, we obtain a bar fraction $f_{bar} \sim 30\% \pm 6\%$. Because of the ambiguity in differentiating

'smooth' disk galaxies from 'pure bulge' galaxies during visual classification (see § 3.2), we also calculate the bar fraction exluding all galaxies classified as 'smooth'. In this case, we obtain a bar fraction $f_{\rm bar} = 44\% \pm 6\%$.

In Figure 6 we show the bar fraction as a function of host galaxy rest-frame M_V luminosity. The bar fraction is calculated for all three methods of disk selection (color cut, sersic cut, and visual classification). In panel (a) the bar fraction remains $\sim 30\%$ within the typical Poisson error of 5-10% in those bins where number statistics are robust ($-20.5 < M_V < -18.5$). In panel (b) and (c) the bar fraction shows a decrease from $36\% \pm 8\%$ at $M_V = -20.5$ to $20\% \pm 4\%$ at $M_V = -18.5$. For panel (c), the brightest bin has enough objects to be statistically significant. If we use all bins from panel (c), we see a decrease in the bar fraction from $48\% \pm 7\%$ at $M_V = -21.5$ to $20\% \pm 4\%$ at $M_V = -18.5$.

To understand the variation of the bar fraction with host galaxy properties, we plot the fraction of bars as a function of morphological class in Figure 7. Here the morphological classes have been grouped by bulge-to-disk ratio in panel (a) and gas/dust content in panel (b). In Fig. 7(a) galaxies with a bulge+disk component are in the first bin of, while pure disk galaxies are in the second bin. We find that the bar fraction increases from $28\% \pm 3\%$ in 'B+D' galaxies to $47\% \pm 5\%$ in 'pure disk' galaxies. The rise in bar fraction as a function of bulge size, or central concentration of the host galaxy is in agreement with BJM08, who found that the bar fraction in pure disk galaxies is a factor of ~ 1.4 higher than in disk galaxies with prominent bulges. This result is further suggested by Figure 7, which shows the bar fraction as a function of central concentration in the host galaxy, as characterized by the effective radius normalized to the disk radius, r_e/a_{disk}. The bar fraction clearly increases with decreasing central concentration, from $17\% \pm 4\%$ in galaxies with high concentration (r_e/a_{disk}=0.15), to $46\% \pm 9\%$ in galaxies with low concentration (r_e/a_{disk}=0.75).

One caveat for the trend of the bar fraction vs. central concentration characterized by r_e/a_{disk} is that the r_e measurement comes from a Sérsic fit to the galaxy. Recent studies have found that the Sérsic index n is preferentially lower in barred galaxies. This in turn may bias r_e/a_{disk} to larger values (lower concentration) for galaxies with bars, thus causing the increase in the bar fraction toward less centrally concentrated galaxies. However, Figure 6 suggests that this effect does not account for the variation in the bar fraction with central concentration, because the same trend is seen when the host galaxy concentration is estimated through visual classification.

In Fig. 7(b) galaxies with no or low gas content ('smooth') are in the first bin, while galaxies that have a lot of gas and dust ('clumpy') are in the second bin. The bar fraction increases from $27\% \pm 3\%$ in gas-poor/'smooth' galaxies, to $44\% \pm 5\%$ in gas-rich/'clumpy'

galaxies. This trend is only underscored by the fact that bars should be harder to identify in gas- and dust-rich galaxies. Clumpy star formation regions and a lot of dust can easily mask the bar signature in the radial profiles of the e and PA. This is the main reason that we find more bars when looking at NIR images of the same galaxies in the local universe (Block et al. 1994; MJ07).

4.4. Bars and Disks on the Red Sequence and Blue Cloud

It is often assumed that the red sequence consists mainly of old, gas-poor, early-type galaxies (e.g., E/S0/Sa). Using our visual morphologies and ellipse-fitting bar classifications, we can investigate the properties of the red sequence and blue cloud galaxies in the STAGES cluster sample.

Most ($\sim 80\%$) of barred galaxies on the red sequence are visually identified as gas-poor 'bulge+disk' galaxies (see Fig. 3(b),(c)), whereas only 4% of galaxies on the blue cloud are visually identified as such. On the blue cloud, the galaxy population is dominated by galaxies visually identified as gas-rich 'bulge+disk', and gas-rich 'pure disk' (see Fig. 3(d),(e) and (f),(g), respectively). Therefore, it is interesting to compare the properties of bars on the red sequence and blue cloud. We find that bars in disks on the red sequence are both larger and weaker (have lower $e_{\rm bar}$ than bars in disks on the blue cloud (Figure 9). We find that the mean semi-major axis of bars on the red sequence (mean $a_{\rm bar} = 3.3\ kpc$) is almost twice that of bars on the blue cloud (mean $a_{\rm bar} = 1.8\ kpc$). The mean bar ellipticity, $e_{\rm bar}$ is 0.75 times smaller for bars on the red sequence (mean $e_{\rm bar} = 0.48$) compared to bars on the blue cloud (mean $e_{\rm bar} = 0.64$). This difference in bar properties between the red sequence and blue cloud can be largely attributed to a difference in galaxy morphology. Because $\sim 80\%$ of red sequence barred galaxies are classified as gas-poor, bulge+disk galaxies, this implies that these types of galaxies on average host larger, weaker bars. Even when normalized to the disk size, red-sequence bars are 1.3 times larger than blue-cloud bars.

To further explore the variation of bar strength (ellipticity) with galaxy morphology, we plot the mean $e_{\rm bar}$ as a function of visual morphological class in Figure 10. We find that the mean bar strength $e_{\rm bar}$ increases from ~ 0.5 in galaxies classified as smooth, bulge+disk to ~ 0.65 in galaxies classified as clumpy, pure disk. This result is in agreement with BMJ08, who also find that pure disk galaxies on average host stronger bars.

4.5. Bar Fraction as Function of Kappa, Σ_{10}, ICM density, and Distance to Nearest Cluster Center

Bars can act as a tool to probe the evolution of galaxies. Frequent tidal interactions can induce stellar bars in dynamically cold disks. However, they may also deplete disks of gas, and tidally heat them, making them less bar unstable. These competing effects are prevalent in cluster environments.

How does the environment density affect the bar fraction, and where do barred galaxies live with respect to the density peaks in the supercluster environment? In this section, we explore these questions using four traces of environment density: the line-of-sight projected surface mass density κ (Heymans et al. 2008), local galaxy number density Σ_{10} (WGM05, Gilmour et al. 2007), ICM density as characterized by the X-ray emission from hot intra-cluster gas, and the projected distance to the nearest cluster center.

Figure 11 shows the variation of the three measures of environment density (κ, Σ_{10}, and ICM density) with distance to the nearest cluster center. It is evident from all three tracers, that density decreases with increasing distance from the nearest cluster center.

Figure 12 shows the variation of the bar (a) and disk (b) fraction as a function of κ. In this plot, the disks are identified through visual classification as outlined in § 3.2. The bars are identified through ellipse-fitting. The bar fraction shows no significant trend with κ within the error bars. The fraction of disk galaxies decreases toward higher densities. When both 'smooth' and 'clumpy' disks are considered, there is a general decrease toward higher κ values from 78%± 3% at $\kappa \sim 0.01$ to 64%± 9% at $\kappa \sim 0.07$.

Figure 13 shows how the bar (a) and disk (b) fraction vary with the local galaxy number density Σ_{10}. Σ_{10} is calculated by finding the radius enclosing the ten nearest neighbors to a galaxy. This is used to calculate a galaxy number density, quoted in $(Mpc/h)^{-2}$. Again, the bar fraction shows no significant trend with Σ_{10}. When 'smooth' and 'clumpy' disks are considered together, their fraction shows a decline toward higher number density from 73%± 4% at $\log(\Sigma_{10})\sim1.7$ $(Mpc/h)^{-2}$ to 44%± 16% at $\log(\Sigma_{10})\sim2.9$ $(Mpc/h)^{-2}$. This decline in the disk fraction towards higher number densities reflects the well-known morphology density relation.

In Figure 14, we plot the bar and disk fractions against ICM density, as characterized by X-ray emission from the hot intra-cluster gas. Again, the bar fraction shows no significant trend with ICM density. When 'smooth' and 'clumpy' disks are considered together, the disk galaxy fraction declines toward higher densities, going from 87%± 6% at 10^{-18} counts s^{-1} to 52%± 11% at $10^{-15.7}$ counts s^{-1}.

Finally, in Figure 15 we plot the variation of the bar and disk fraction as a function of the distance to the nearest cluster $D_{\rm min}$. This is a more indirect measurement of the local density, based on the assumption that galaxies at small distances from any of the clusters are at the moment occupying a higher-density environment than galaxies at large distances from any of the cluster centers. Over the bins where we have good number statistics, the bar fraction remains $\sim 30\%$ within the typical error of $\sim 5\%$ out to $D_{\rm min} \sim 1.4$ Mpc, and then drops to $14\% \pm 7\%$ at $D_{\rm min} \sim 1.8$ Mpc. The fraction of 'smooth' and 'clumpy' disks (solid line in panel (b)) decreases with decreasing $D_{\rm min}$ from $86\% \pm 5\%$ at $D_{\rm min} \sim 1.4$ Mpc to $66\% \pm 4\%$ at $D_{\rm min} \sim 0.2$ Mpc.

4.6. Comparison to the Field

To understand what impact cluster processes have on the evolution of bars and disk galaxies, we must compare their properties to galaxies unaffected by such processes found in low density environments. We compare the results on bars and disks from the STAGES sample to those from the Ohio State University Bright Spiral Galaxy Survey (OSUBSGS; Eskridge et al. 2002) and the Sloan Digital Sky Survey (SDSS; REF). Specifically, we use the results of MJ07 and BJM08, where bars are identified and characterized through ellipse-fits, and analysis was performed in the same way as for the STAGES sample. Before we compare the results obtained for bars in the cluster with those from the field studies, we must determine if the underlying galaxy populations in the samples are the same. Figure 16 shows the absolute $M_{\rm V}$ magnitude (a) and rest-frame U-V color (b) distributions of the STAGES and OSUBSGS samples. It is evident that the OSUBSGS sample is made up of both brighter and bluer galaxies than the cluster sample. Figure 17 shows the mass distributions of STAGES and OSU sample. Both samples have similar ranges in mass, but the OSU sample contains slightly more massive galaxies on average. These are important caveats to keep in mind for the following analysis.

Figure 18 shows the stellar mass distributions of the STAGES and SDSS sample. The two samples have similar distributions in stellar mass, peaking at $\sim 10^{9}.5\ M/M_{\odot}$, however the STAGES distribution is wider, and contains galaxies down to $10^{8}\ M/M_{\odot}$ and up to $10^{12}\ M/M_{\odot}$. SDSS galaxies are found mostly in the range $10^{9} - 10^{10.5}\ M/M_{\odot}$. For this reason, in the comparison of the results of the STAGES and SDSS studies, we only consider galaxies in the range $10^{9} - 10^{10.5}\ M/M_{\odot}$.

4.6.1. Bar Fraction

The bar fraction in STAGES is found to be $\sim 30\% \pm 6\%$ for all methods of disk selection. The optical bar fraction in OSUBSGS is $44\% \pm 7\%$ (MJ07), and in the SDSS it is 48%–52% (BJM08). Thus we find that, within the uncertainty, the bar fraction in the STAGES cluster sample is comparable to that in the field samples. This suggests that the formation and/or destruction of a bar is strongly influenced by the properties of the host disk itself rather than on large-scale environmental effects.

4.6.2. Bar Size and Strength Distribution

Figure 19 shows the bar size $a_{\rm bar}$ (a) and peak ellipticity $e_{\rm bar}$ (b) distributions for the STAGES and OSUBSGS samples. The two samples have a similar distribution in $a_{\rm bar}$, however the OSUBSGS sample is weighted toward higher bar ellipticities. This could be a result of the fact that the OSUBSGS sample is bluer than the STAGES sample (Figure 16), combined with the fact that bluer, later-type disks tend to host stronger bars (see § 4.4 and Figure 9).

To compare the bar properties of the STAGES cluster sample to those found in SDSS, first we select galaxies from both samples in the same mass range $M/M_{\odot} \sim 10^{9} - 10^{10.5}$. The resulting $a_{\rm bar}$ and $e_{\rm bar}$ distributions are plotted in Figure 20. The bar size and strength distributions of the two samples agree fairly well, with the STAGES $e_{\rm bar}$ distribution weighted toward slightly higher ellipticities. This result is interesting, in light of the fact that the SDSS sample is selected using a color cut (i.e., selecting only blue-cloud galaxies; BJM08), while no color cut is taken in this case for the STAGES galaxies. Since both studies find that bars on the blue cloud are stronger on average than bars on the red sequence, we should expect the SDSS $e_{\rm bar}$ distribution to be weighted toward larger ellipticities, however this is not the case. This result points to a difference in the galaxies that populate the blue cloud in the supercluster vs. the SDSS field.

5. Summary and Conclusions

We have used the STAGES HST ACS survey of the Abell 901/902 supercluster at z$\sim$0.165 to study the properties of barred and unbarred disks in a dense environment. Ellipse-fitting was used to identify and characterize the properties of bars in our sample, as well as visual classification for an extra check. We characterized the morphologies of the cluster galaxies using visual classification. Galaxies were grouped according to a broad classification

of bulge-to-disk ratio into the classes: 'pure bulge', 'bulge+disk', and 'pure disk'. In addition, the gas content of the galaxies was classified by looking at whether the galaxy appeared mostly 'clumpy'/gas-rich, or mostly 'smooth'/gas-poor. To identify the bar fraction $f_{\rm bar}$, three methods of disk selection were used and compared: visual classification, color cut, and Sérsic cut. Using our sample of 487 moderately inclined ($i < 60°$), ellipse-fitted, bright ($M_{\rm V} \leq$ -18), cluster galaxies, we find the following results.

1. *Disk selection in clusters:* The traditional methods of disk selection such as taking a color cut or Sérsic cut, are problematic in a cluster environment. In dense environments, bulge-dominated, red disks are prevalent, so many disk galaxies may be missed by selecting only blue-cloud galaxies, or those with Sérsic $n < 2.4$. We use our visual morphological classifications to investigate the validity of these two disk selection methods and find that a color cut misses 24% – 54% of disk galaxies on the red sequence, and a Sérsic cut misses 24% – 37% of disk galaxies with $n > 2.5$. The uncertainty comes from the ambiguity in visually distinguishing 'pure bulge' galaxies from 'bulge+disk smooth' galaxies. Therefore, a blind application of a color cut or Sérsic cut would miss many red, bulge-dominated galaxies that are prevalent in a cluster environment.

2. *Bar fraction as a function of host galaxy properties:* For all three methods of disk selection (visual, color cut, sersic cut), we obtain a bar fraction $f_{\rm bar} \sim 30\% \pm 6\%$. We find that the fraction of bars increases towards brighter galaxies from 20%± 4% at $M_{\rm V}$ = -18.5 to 48%± 7% at $M_{\rm V}$ = -21.5 when visual classification is used to select disk galaxies. The trend is weaker when a Sérsic cut is used to select disks, and not present when a color cut is used. The bar fraction is a factor of ~ 1.8 higher in galaxies classified as 'pure disk' compared to galaxies visually classified as 'bulge+disk'. When the normalized effective radius $r_{\rm e}/a_{\rm disk}$ is used to trace central galaxy concentration, the bar fraction is ~ 2.7 times higher in galaxies with the lowest central concentration ($r_{\rm e}/a_{\rm disk} = 0.75$) compared to the galaxies with the highest central concentration ($r_{\rm e}/a_{\rm disk} = 0.15$). This result is in agreement with BJM08. We also find that the bar fraction is ~ 1.6 times higher in 'clumpy' galaxies than in galaxies that appear 'smooth'. Taken together, these results imply that it is easier to form and/or sustain a bar in galaxies with low central concentration and high gas content.

3. *Bars and disks on the red sequence and blue cloud:* We find that $\sim 80\%$ of barred disks on the red sequence are identified as 'bulge+disk smooth' galaxies. On the blue cloud, the barred galaxy population is dominated by 'clumpy'/gas-rich 'bulge+disk' and 'pure disk' galaxies. Comparing the properties of bars on the red sequence and blue cloud, we find that the mean semi-major axis ($a_{\rm bar}$ of red-sequence bars is ~ 1.3 times as large as that of blue cloud bars, when normalized to the disk sizes of the host

galaxies. Bars in blue cloud galaxies are also ~ 1.3 times stronger on average than bars in red sequence galaxies. When the mean bar strength or ellipticity is plotted vs. visual morphological type, the $e_{\rm bar}$ increases from 0.5 in 'bulge+disk smooth' galaxies to 0.65 in 'pure disk clumpy' galaxies. This implies that 'bulge+disk smooth' or S0/a-type galaxies host on average larger, weaker bars than later-type spirals, in agreement with BJM08 and Laurikainen et al. 2007.

4. *Bar fraction as a function of κ, Σ_{10}, ICM density, and distance from nearest cluster center:* We find no trend of the fraction of barred disks with any of the four traces of environment density. We investigate the fraction of disk galaxies as a function of environment density. The fraction of disk galaxies, as determined from visual classification, declines steadily from low to high local densities in the supercluster. When the fraction of 'clumpy/dusty' galaxies is considered, we recover the well-known morphology-density relation.

5. *Comparison to field studies:* We compare our results to those for field samples, specifically MJ07 (OSUBSGS) and BJM08 (SDSS) where bar identification and characterization was done in the same way as for the STAGES sample. The bar fraction in the cluster, $f_{\rm bar,STAGES} \sim 30\% \pm 6\%$ is comparable to the optical bar fraction found for field galaxies (e.g., $f_{\rm bar,field} \sim 44\% \pm 6\%$) within the range of uncertainty. This implies that the processes that affect bar formation and destruction are overwhelmingly dictated by particular properties of the host galaxy, and not the local environment in which the galaxy currently lives.

S.J. and I.M. acknowledge .....

REFERENCES

Abraham, R. G., et al. 1996, ApJ, 471, 694

Athanassoula, E. 1992b, MNRAS, 259, 345

Balogh, M. L., Navarro, J. F., & Morris, S. L. 2000, ApJ, 540, 113

Bekki, K. 1999, ApJL, 510, L15

Bell, E. F., et al. 2004, ApJ, 608, 752

Binggeli, B., Sandage, A., & Tammann, G. A. 1988, ARAA, 26, 509

Borch, A., et al. 2006, A&A, 453, 869

Butcher, H., & Oemler, A., Jr. 1978, ApJ, 219, 18

Byrd, G., & Valtonen, M. 1990, ApJ, 350, 89

Dubinski, J., Gauthier, J.-R., Widrow, L., & Nickerson, S. 2008, ArXiv e-prints, 802, arXiv:0802.3997

Elmegreen, B. G., Elmegreen, D. M., & Hirst, A. C. 2004, ApJ, 612, 191

Evrard, A. E., Silk, J., & Szalay, A. S. 1990, ApJ, 365, 13

Fisher, D. B. 2006, ApJL, 642, L17

Friedli, D., Wozniak, H., Rieke, M., Martinet, L., & Bratschi, P. 1996, A&A Suppl., 118, 461

Gray, M. E., Taylor, A. N., Meisenheimer, K., Dye, S., Wolf, C., & Thommes, E. 2002, ApJ, 568, 141

Gunn, J. E., & Gott, J. R. I. 1972, ApJ, 176, 1

Hernquist, L., & Mihos, J. C. 1995, ApJ, 448, 41

Jogee, S. 1999, Ph.D. thesis, Yale University

Jogee, S., Knapen, J. H., Laine, S., Shlosman, I., Scoville, N. Z., & Englmaier, P. 2002a, ApJL, 570, L55

Jogee, S., Shlosman, I., Laine, S., Knapen, J. H., Englmaier, P., Scoville, N. Z., & Wilson, C. D. 2002b, ApJ

Jogee, S., Barazza, F., Rix, H.-W., Shlosman, I. et al. 2004a, ApJl, 615, L105

Knapen, J. H., Shlosman, I., & Peletier, R. F. 2000, ApJ, 529, 93

Kodama, T., & Smail, I. 2001, MNRAS, 326, 637

Koopmann, R. A., & Kenney, J. D. P. 1998, ApJL, 497, L75

Kormendy, J. 1982, ApJ, 257, 75

Kormendy, J. 1993, Galactic Bulges, 153, 209

Lacey, C., & Silk, J. 1991, ApJ, 381, 14

Laine, S., Shlosman, I., Knapen, J. H., & Peletier, R. F. 2002, ApJ, 567, 97

Larson, R. B., Tinsley, B. M., & Caldwell, C. N. 1980, ApJ, 237, 692

Marinova, I., & Jogee, S. 2007, ApJ, 659, 1176

Méndez-Abreu, J., Aguerri, J. A. L., & Corsini, E. M. 2008, ArXiv e-prints, 802, arXiv:0802.0011

Menéndez-Delmestre, K., Sheth, K., Schinnerer, E., Jarrett, T. H., & Scoville, N. Z. 2007, ApJ, 657, 790

Moore, B., Katz, N., Lake, G., Dressler, A., & Oemler, A. 1996, Nature, 379, 613

Moore, B., Lake, G., & Katz, N. 1998, ApJ, 495, 139

Mulchaey, J. S., & Regan, M. W. 1997, ApJL, 482, L135

Oemler, A. J. 1974, ApJ, 194, 1

Regan, M. W., Vogel, S. N., & Teuben, P. J. 1997, ApJ, 482, L143

Sheth, K., Regan, M. W., Scoville, N. Z., & Strubbe, L. E. 2003, ApJL, 592, L13

Treu, T., Ellis, R. S., Kneib, J.-P., Dressler, A., Smail, I., Czoske, O., Oemler, A., & Natarajan, P. 2003, ApJ, 591, 53

Wolf, C., et al. 2004, A&A, 421, 913

Wolf, C., Gray, M. E., & Meisenheimer, K. 2005, A&A, 443, 435

Wozniak, H., Friedli, D., Martinet, L., Martin, P., & Bratschi, P. 1995, A&A Suppl., 111, 115

Zabludoff, A. I., & Franx, M. 1993, AJ, 106, 1314

Table 1. Bar Fractions and Disk Selection ($M_V \leq -18$)

Method	N_{disk}	N_{bar}	f_{bar}
Visual	360	116	32% ± 6%
Color	184	54	29% ± 6%
Sérsic	262	73	28% ± 6%

Note. — All bar fractions are for galaxies with $M_V \leq$ -18. Columns are : (1) Method of disk galaxy selection; (2) Number of disks; (3) Number of bars. Bars are detected through ellipse fitting. (4) Bar fraction.

Table 2. Bar Fractions and Disk Selection ($\log(M/M_\odot > 9)$)

Method	N_{disk}	N_{bar}	f_{bar}
Visual	418	131	31% ± 6%
Color	201	63	31% ± 6%
Sérsic	326	89	27% ± 6%

Note. — All bar fractions are for galaxies with $\log(M/M_\odot) > 9$. Columns are : (1) Method of disk galaxy selection; (2) Number of disks; (3) Number of bars. Bars are detected through ellipse fitting. (4) Bar fraction.

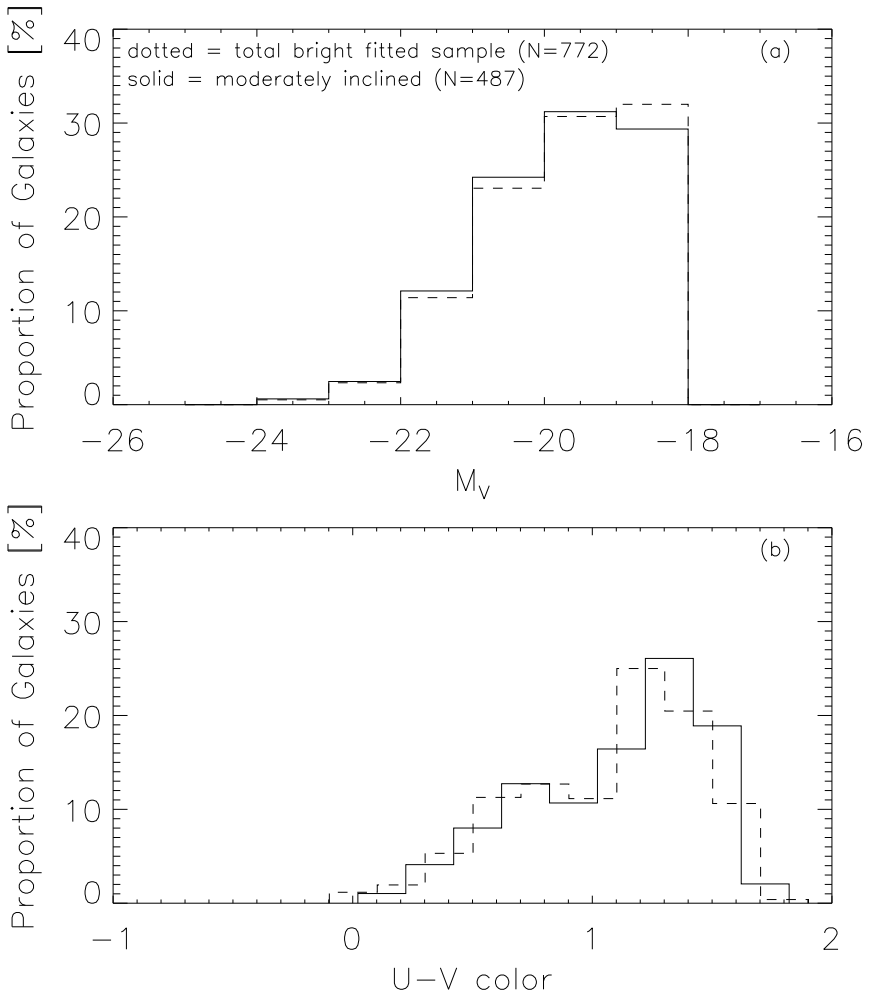

Fig. 1.— (a) The dotted line shows the histogram of M_V luminosity of our cluster sample of 772 ellipse-fitted, bright ($M_V \leq -18$) galaxies. Most galaxies have $-20 \leq M_V \leq -18$. The solid line shows the M_V distribution of the final cluster sample, after excluding highly inclined ($i > 60°$), and poorly fitted galaxies. (b) Rest-frame U-V color distribution of the whole ellipse-fitted sample of 772 galaxies (dotted line) and final sample, after excluding highly inclined galaxies and bad fits (487 galaxies; solid line). Excluding the highly inclined galaxies does not have a significant effect on the absolute M_V magnitude, or rest-frame U-V color distributions.

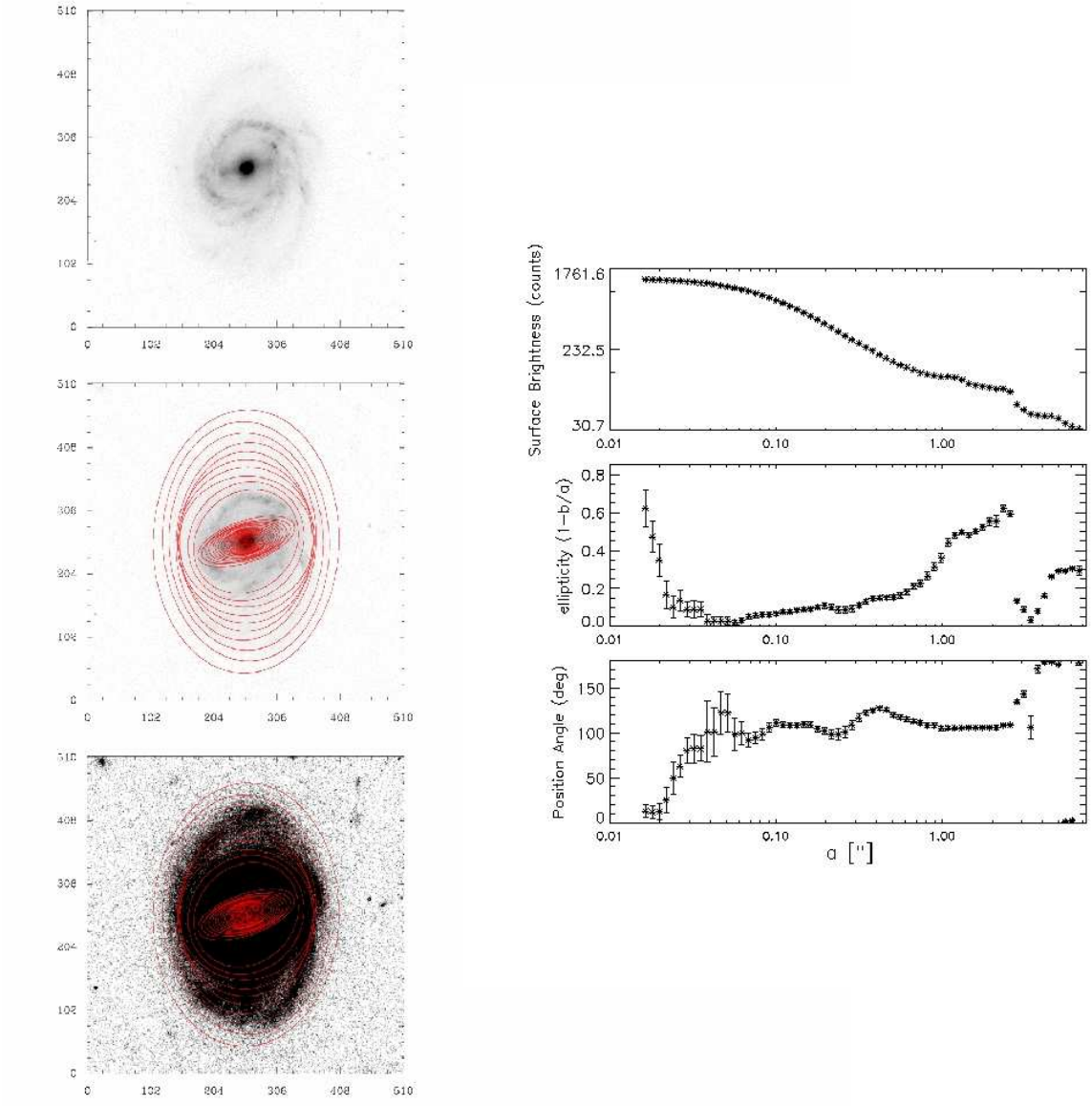

Fig. 2.— *Left*: Ellipse fit overlays on the image of a barred cluster galaxy. In the middle and bottom panels, the contrast is adjusted to show the inner regions and outer disk regions, respectively. *Right*: Radial profiles of the SB, e, and PA. The bar signature is evident in the smooth rise of the e to a global maximum, while the PA remains relatively constant in the bar region. The e then drops and the PA changes, indicating the transition to the disk region.

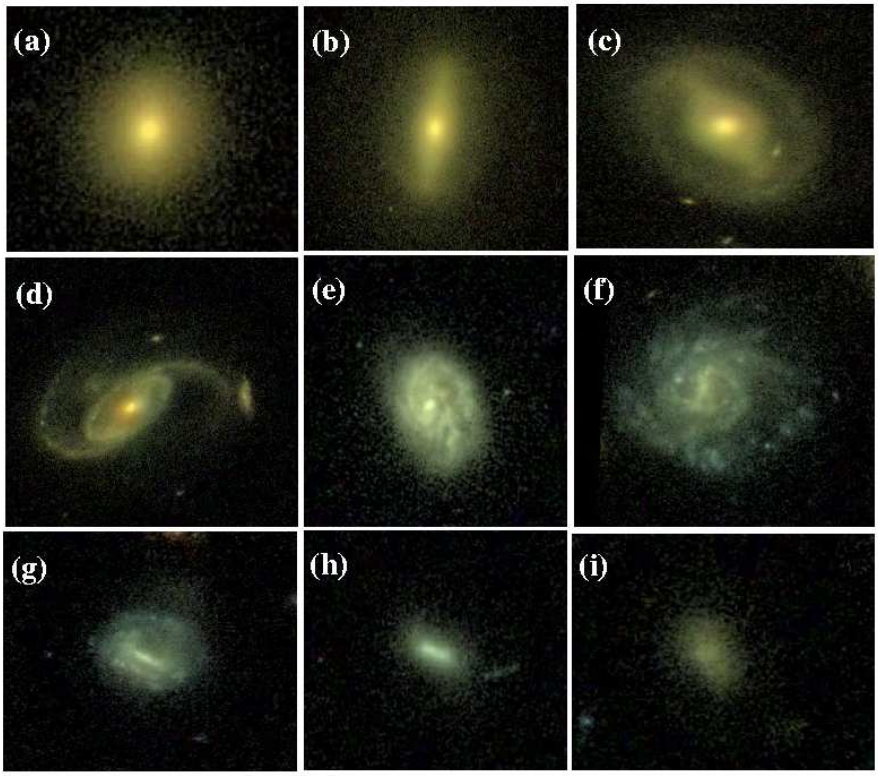

Fig. 3.— Examples of the visual morphological classes used to characterize cluster galaxies. Panel (a) shows an example of the class 'pure bulge'. Panels (b) and (c) show examples of 'bulge+disk smooth' galaxies, while panels (d) and (e) show examples of 'bulge+disk clumpy' galaxies. Panels (f) and (g) show 'pure disk clumpy' galaxies, and panels (h) and (i) show galaxies classified as 'pure disk smooth'.

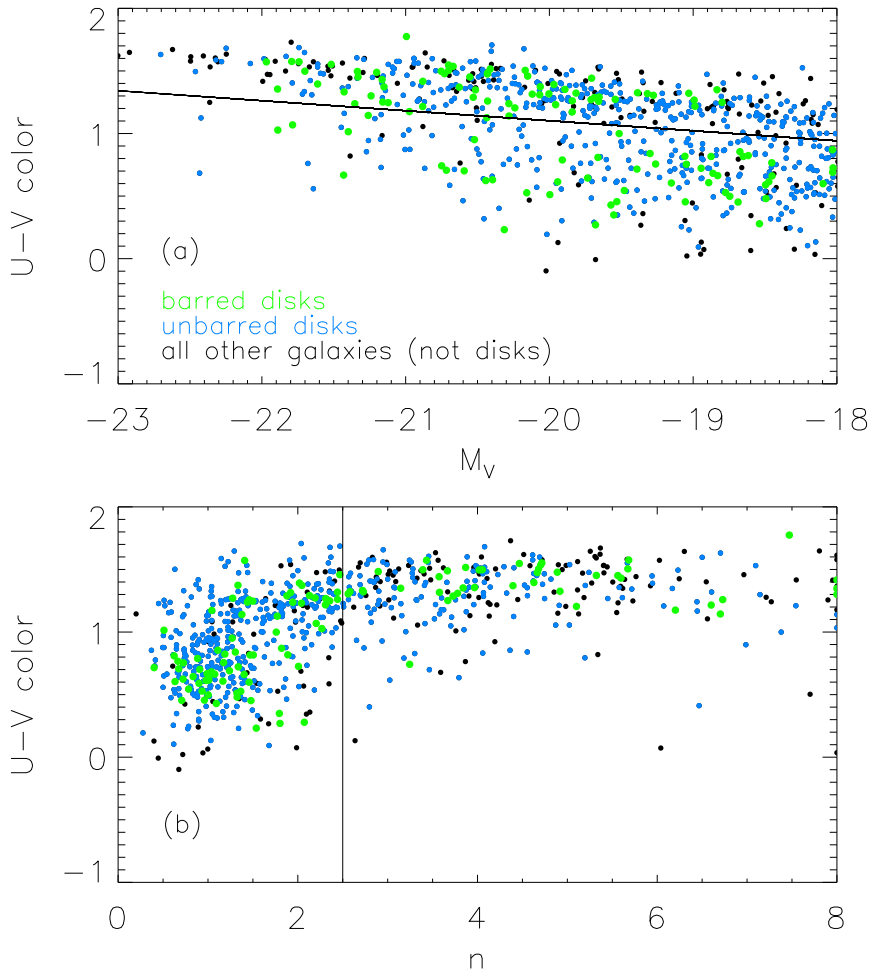

Fig. 4.— (a) We plot the rest-frame U-V color vs. M_V magnitude. The blue points denote galaxies identified as disks using visual classification (§ 3.2), while the black points represent all other galaxies, not classified as disks. Barred disks are shown as the large green points. The solid line separates the red sequence from the blue cloud galaxies. A color cut selecting disks only below this line would miss 24% – 54% of disk galaxies on the red sequence. (b) We plot the rest-frame U-V color vs. Sérsic index, n. The solid line shows the cutoff of n=2.5, which is supposed to separate disk galaxies and spheroids. Again, if such a cut is used to select disks, many visually identified disk galaxies (24% – 37%) with n> 2.5 are missed.

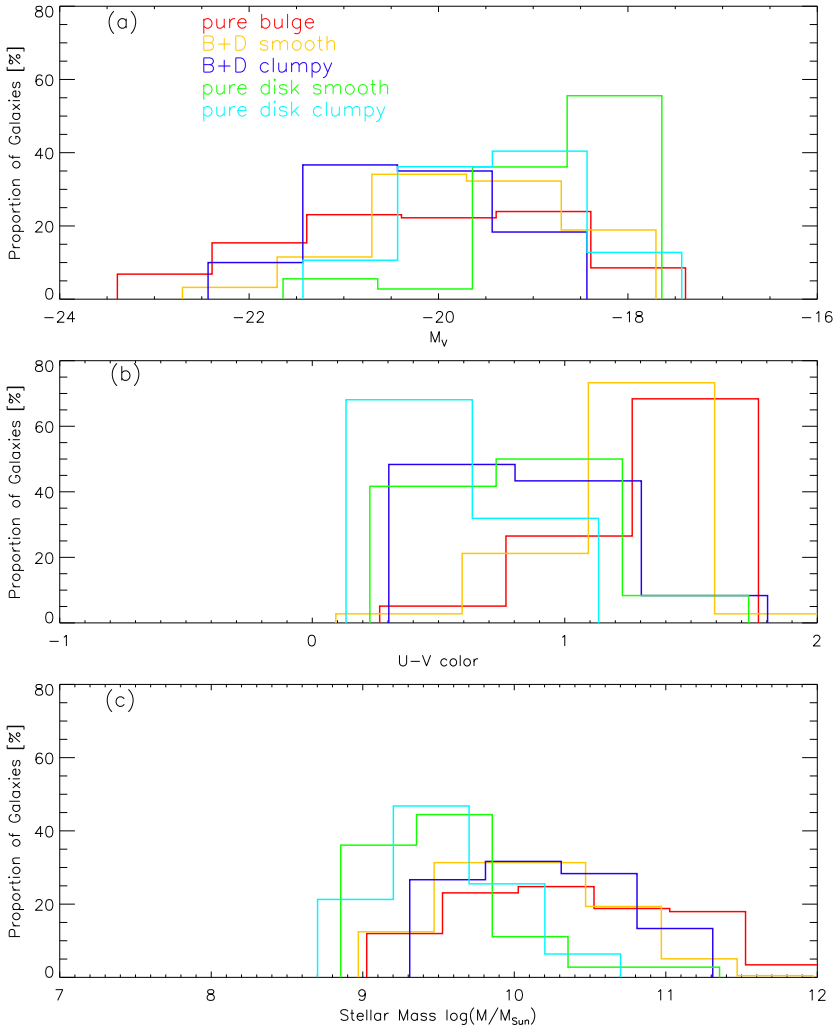

Fig. 5.— (a) Absolute M_V magnitude distributions of the five visual morphological classes in the moderately-inclined, fitted sample. 'bulge+disk clumpy' galaxies have the highest average M_V of -20.5 mag, while 'pure bulge' galaxies occupy the whole range in M_V. As expected, late-type 'pure disk' galaxies are at the faint end, with $M_V \sim$ -19. (b) Rest-frame U-V color distributions of the visual morphological classes. 'Pure bulge' and 'bulge+disk smooth' galaxies are the reddest, while 'pure disk clumpy' are the bluest, as expected from the galaxy properties of the traditional Hubble Sequence. (c) Stellar mass distributions of the visual morphological classes. As expected, the visual classes comprised mostly of giant galaxies ('pure bulge', 'bulge+disk smooth', and 'bulge+disk clumpy') have higher masses, while galaxies classified as 'pure disk clumpy' (e.g., Sc-Sm) and 'pure disk smooth' galaxies are at the lower-mass end.

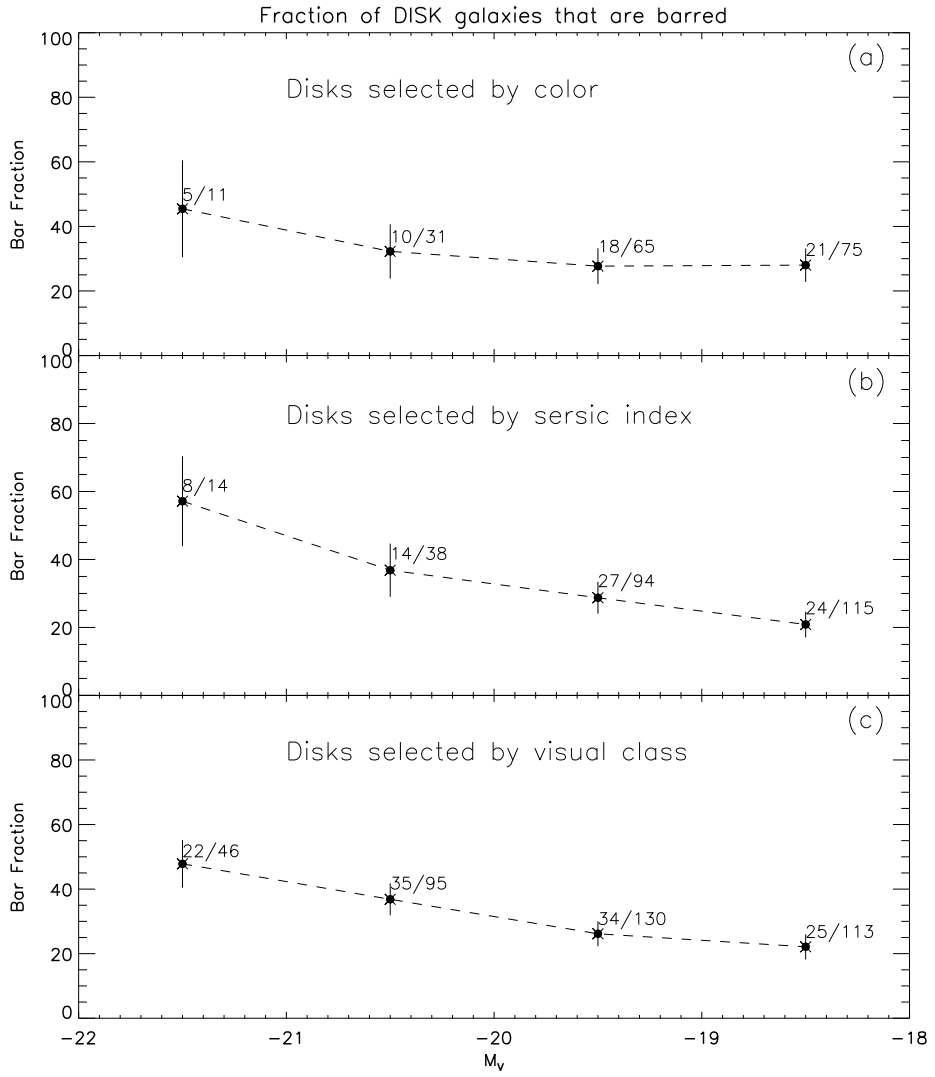

Fig. 6.— We plot the bar fraction as a function of galaxy luminosity M_V for the three methods of disk selection. (a) Disks are selected by a color cut. (b) Disks are selected by a Sérsic cut, picking out galaxies with n$\leq$ 2.5. (c) Disks are selected through visual classification, using the criteria outlined in § 3.2. The strongest trend is seen in panel (c) where the bar fraction decreses from 48%± 7% at M_V = -21.5 to 20%± 4% at M_V = -18.5. Panel (b) shows a decrease in the bar fraction from 36%± 8% at M_V = -20.5 to 20%± 4% at M_V = -18.5 (the bins where number statistics are robust). There is no trend seen in panel (a) within the typical Poisson errors of $\sim$ 5-10%.

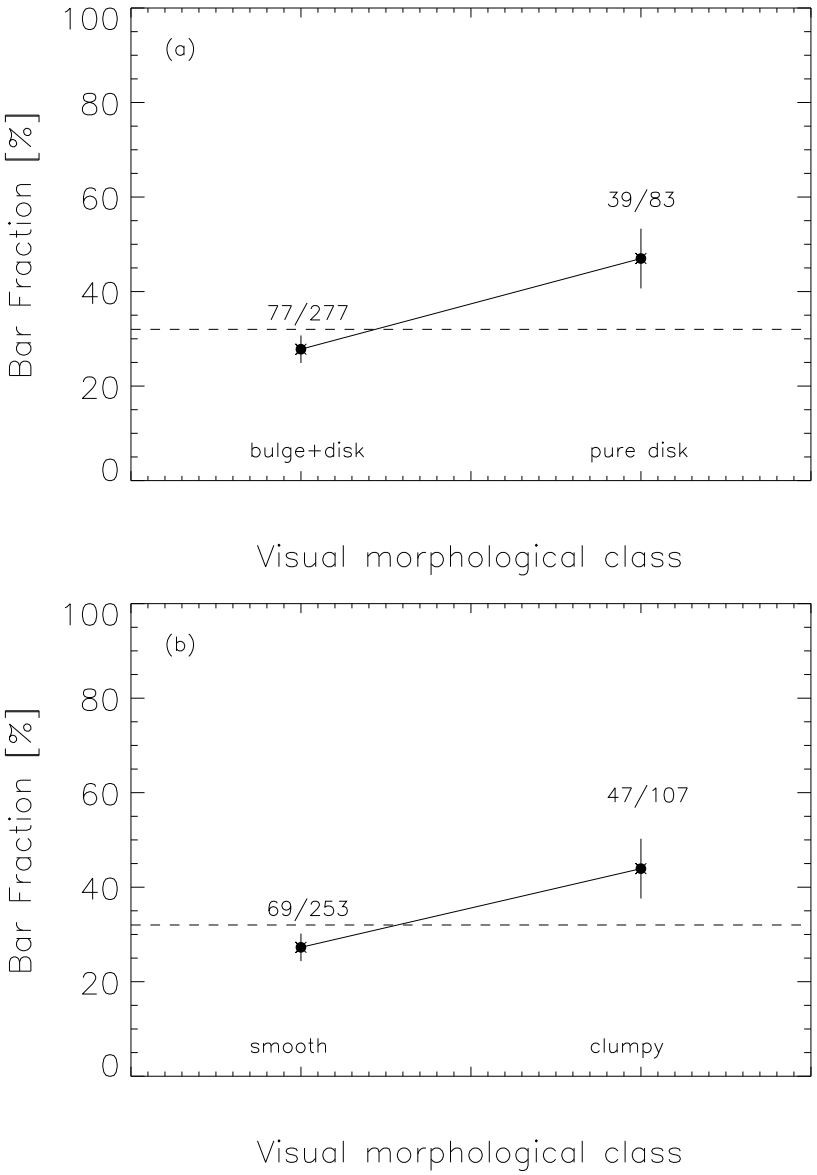

Fig. 7.— The bar fraction as a function of visual morphological class. The total bar fraction (32%± 6%) using visual disk selection is shown as the horizontal dashed line in both panels. In panel (a), the first bin contains galaxies classified as 'bulge+disk', while the second bin contains galaxies classified as 'pure disk'. The bar fraction shows a rise from 28%± 3% to 47%± 5% from galaxies classified as 'bulge+disk' to 'pure disk'. In panel (b), the first bin contains galaxies classified as 'smooth'/gas-poor and the second bin contains 'clumpy'/gas-rich galaxies. The bar fraction increases from 27%± 3% in gas-poor/'smooth' galaxies, to 44%± 5% in gas-rich/'clumpy' galaxies.

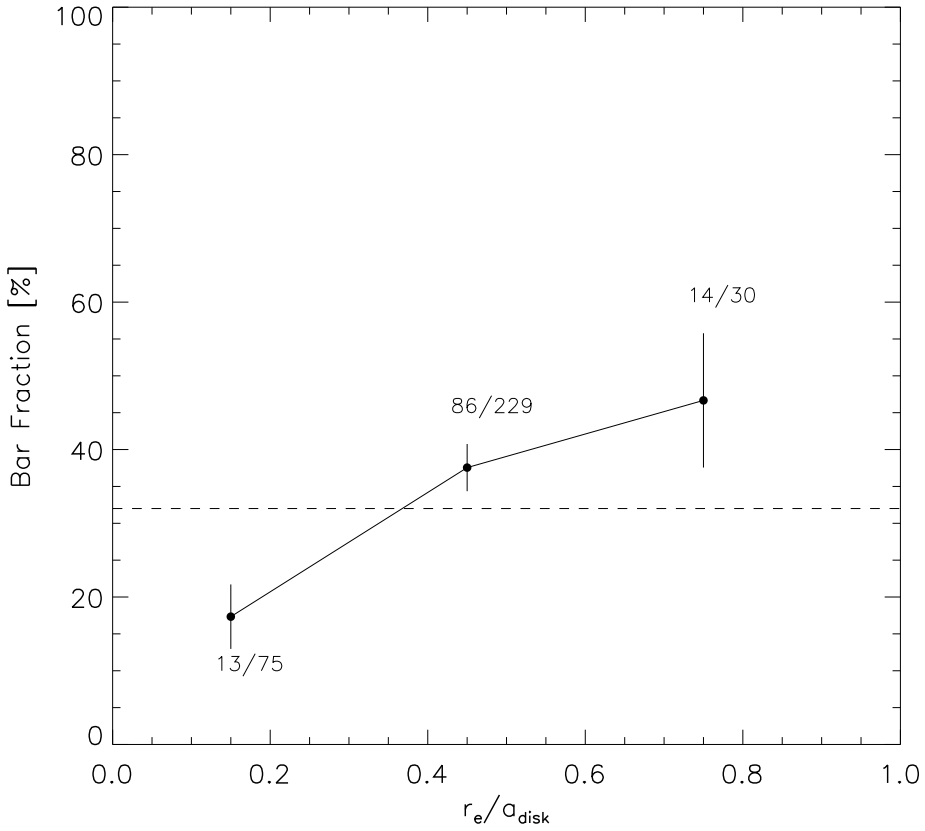

Fig. 8.— The bar fraction as a function of central galaxy concentration, as characterized by the effective radius normalized to the disk radius, $r_{\rm e}/a_{\rm disk}$. Only bins with significant number statistics are shown. The bar fraction increases from 17%± 4% in galaxies with high concentration ($r_{\rm e} \sim 0.15$), to 46%± 9% in galaxies with low concentration ($r_{\rm e} \sim 0.75$).

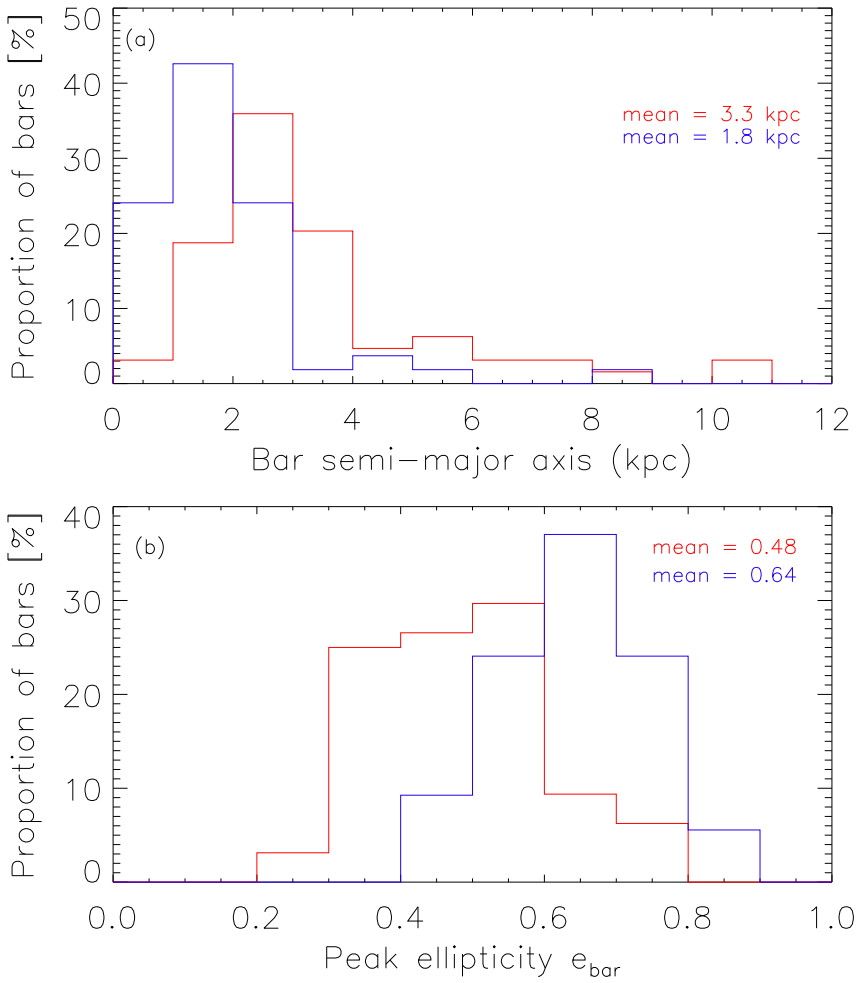

Fig. 9.— The semi-major axis, $a_{\rm bar}$, and peak ellipticity, $e_{\rm bar}$, distributions of bars on the red sequence (red line) and blue cloud (blue line). The average $a_{\rm bar}$ of bars on the red sequence is twice as large as for bars on the blue cloud. The average $e_{\rm bar}$ of red-sequence bars is smaller by 0.75 compared to the $e_{\rm bar}$ of bars on the blue cloud.

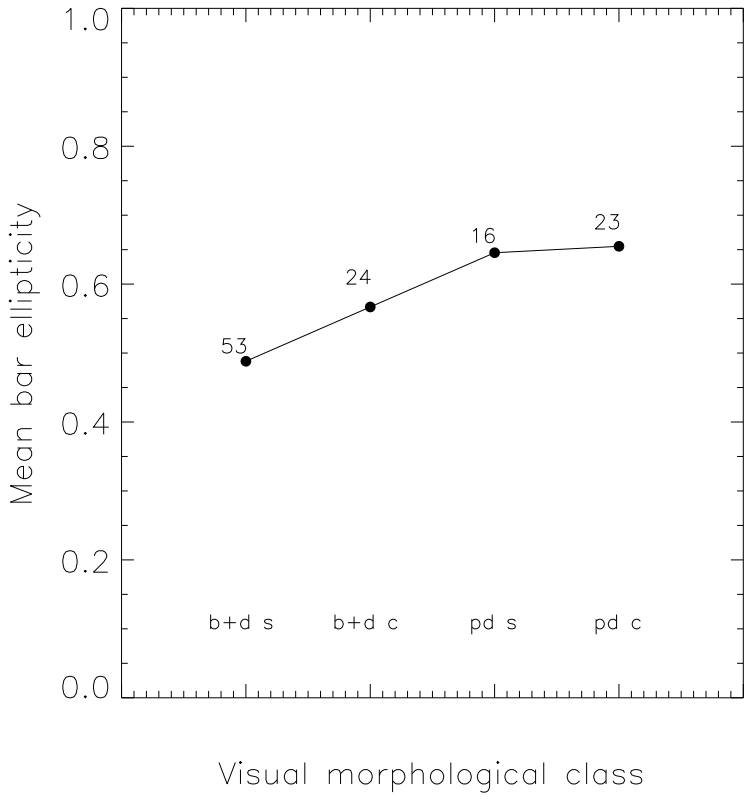

Fig. 10.— The mean bar ellipticity ($e_{\rm bar}$) as a function of visual morphological class. The number of galaxies is shown above each bin. The bar ellipticity is higher in galaxies classified as pure disk ($e_{\rm bar} \sim 0.65$), than in galaxies classified as having a bulge component ($e_{\rm bar} \sim 0.5$).

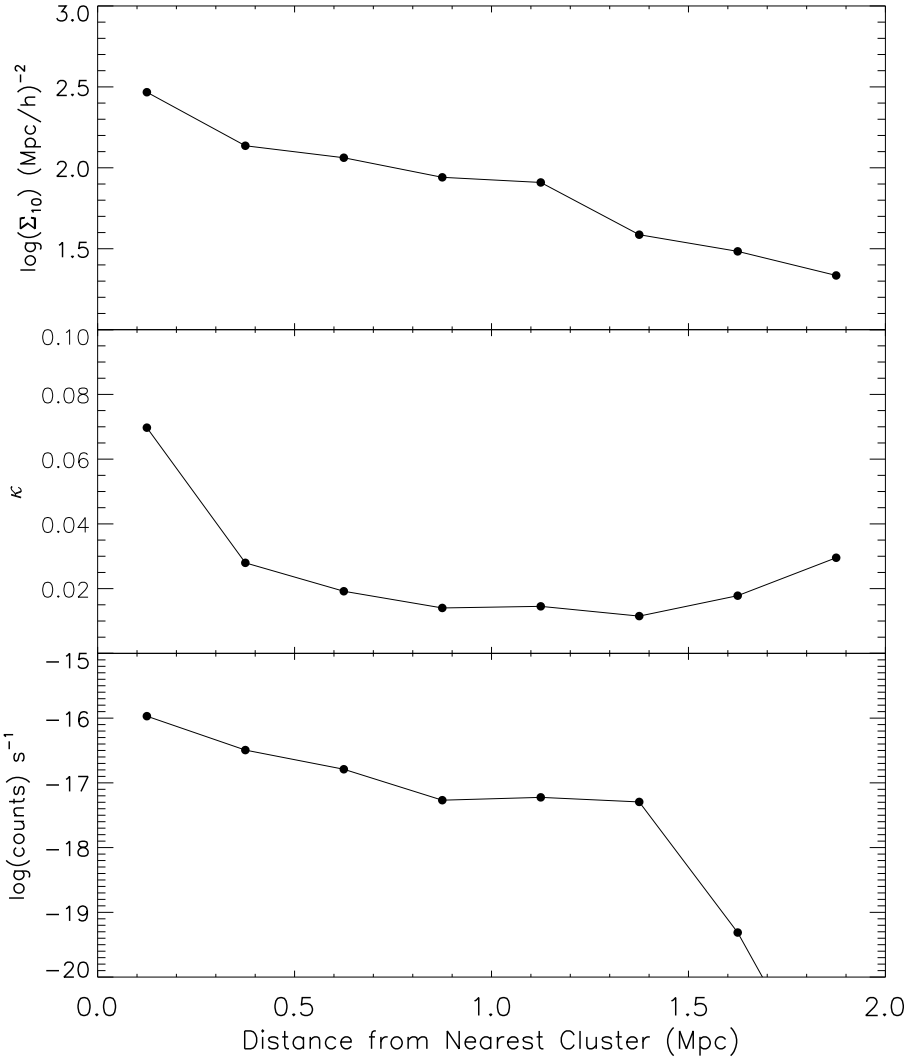

Fig. 11.— We plot the variation of the three measures of environment density (κ, Σ_{10}, ICM density) as a function of distance to the nearest cluster center.

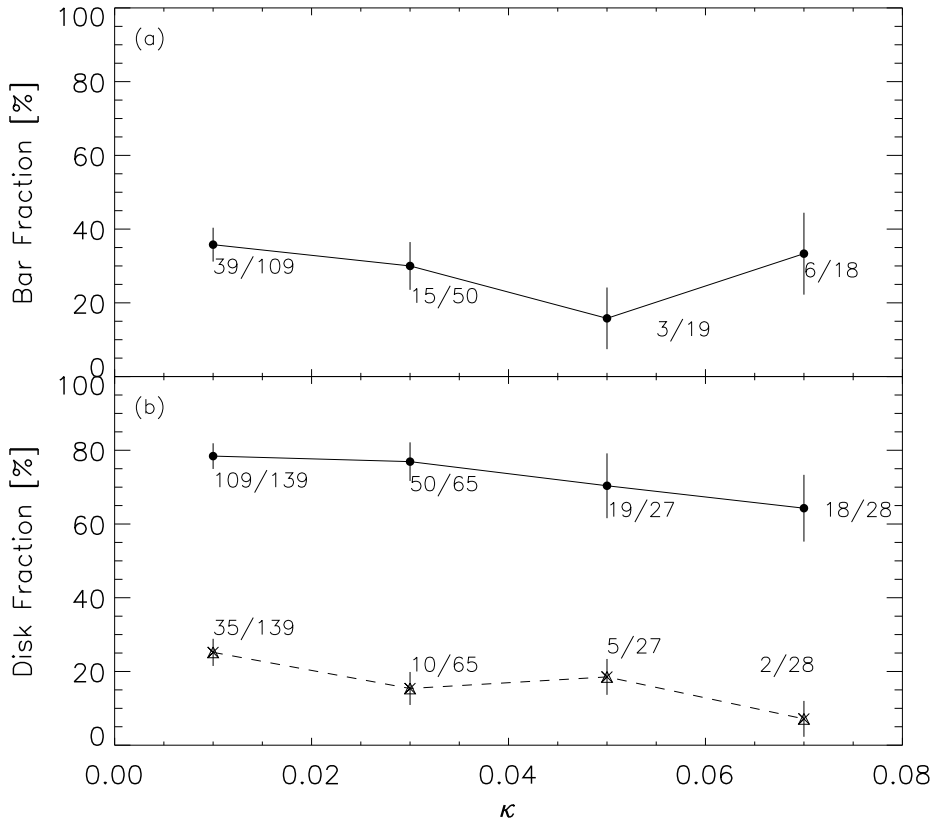

Fig. 12.— (a) The fraction of barred galaxies as a function of local projected mass density, κ. Bars are identified through ellipse-fitting. (b) The fraction of disk galaxies as a function of κ. Disks are identified through visual classification. The solid line shows the fraction of both 'smooth' and 'clumpy' disks, while the dashed line shows only the fraction of 'clumpy' disks.

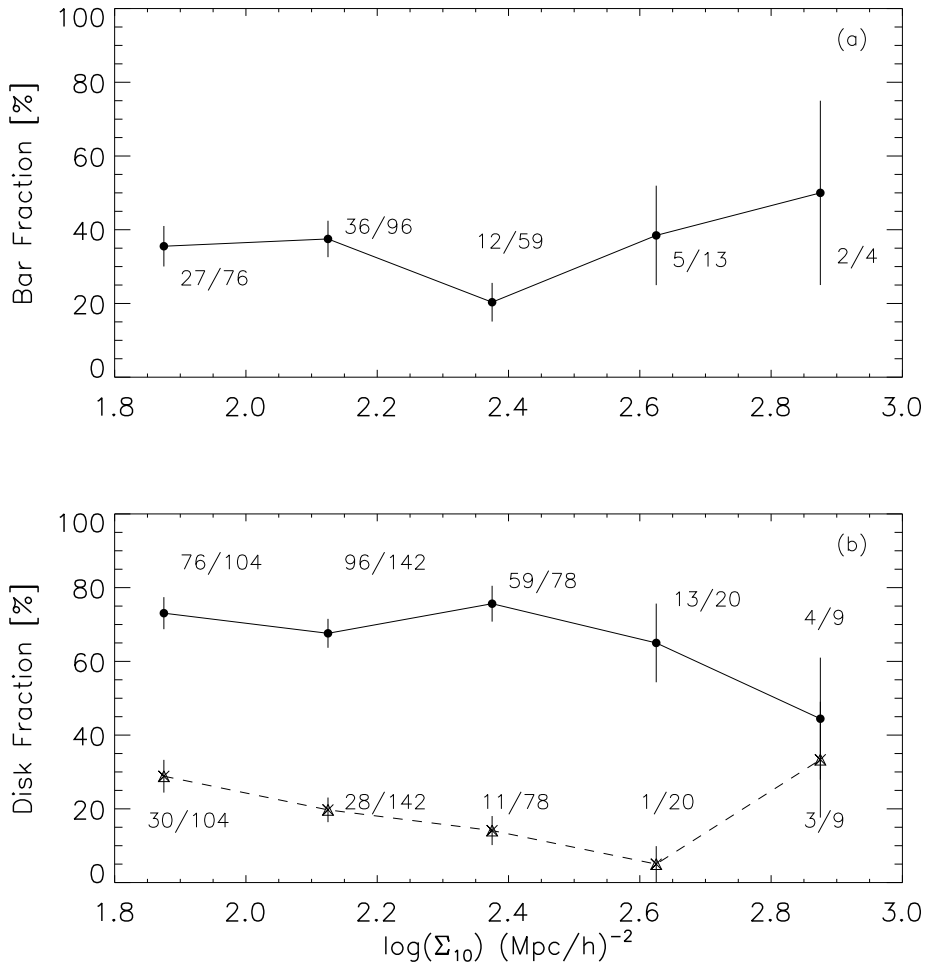

Fig. 13.— (a) The fraction of barred galaxies as a function of local galaxy number density, Σ_{10}. Bars are identified through ellipse-fitting. (b) The fraction of disk galaxies as a function of Σ_{10}. Disks are identified through visual classification. The solid line shows the fraction of both 'smooth' and 'clumpy' disks, while the dashed line shows only the fraction of 'clumpy' disks.

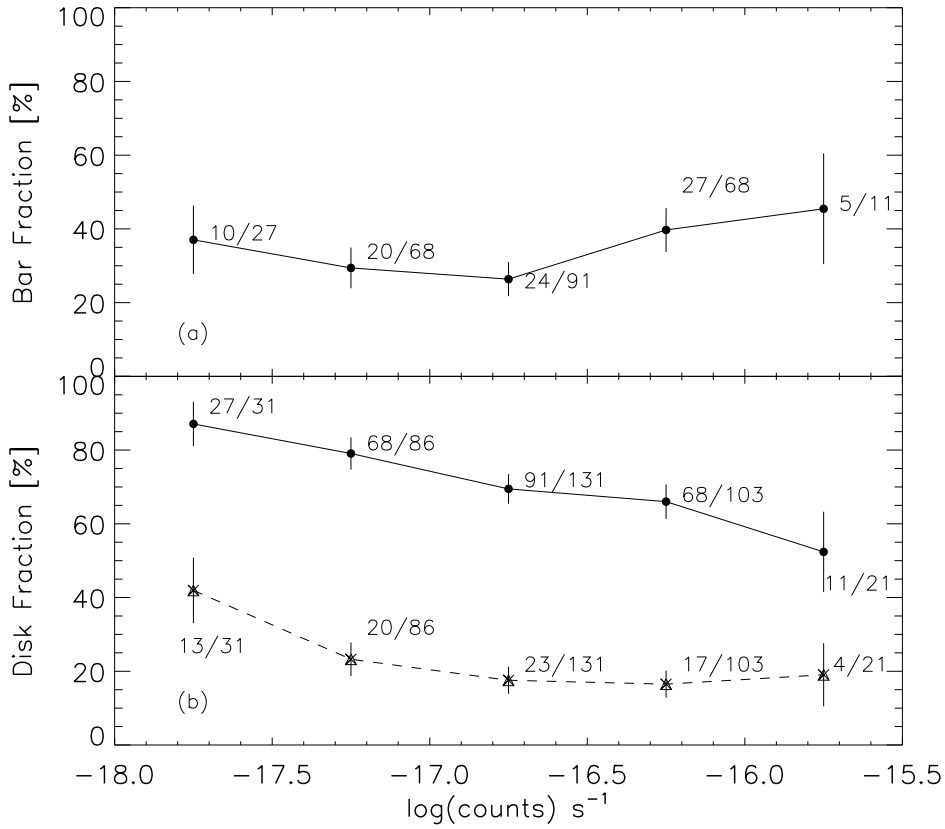

Fig. 14.— (a) The fraction of barred galaxies as a function of ICM density, as traced by the X-ray emission from hot gas. Bars are identified through ellipse-fitting. (b) The fraction of disk galaxies as function of ICM density. Disks are identified through visual classification. The solid line shows the fraction of both 'smooth' and 'clumpy' disks, while the dashed line shows only the fraction of 'clumpy' disks.

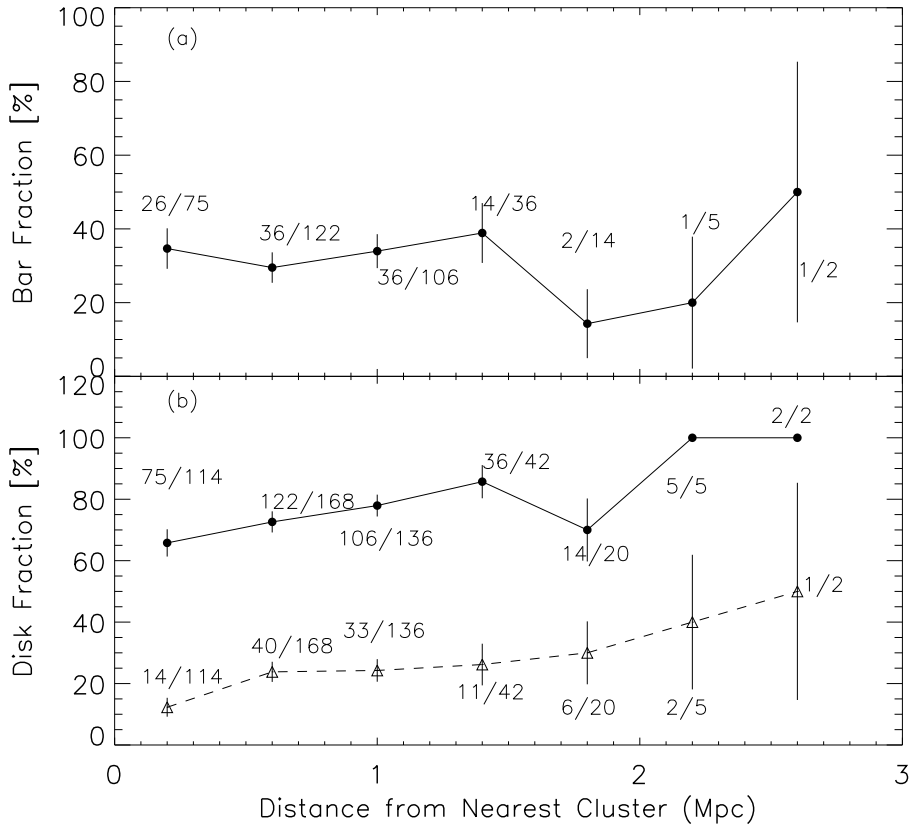

Fig. 15.— (a) The fraction of barred galaxies as a function of the distance from the nearest cluster center in Mpc. (b) The disk fraction as a function of the distance from the nearest cluster center in Mpc. Disks are identified through visual classification. The solid line shows the fraction of both 'smooth' and 'clumpy' disks, while the dashed line shows only the fraction of 'clumpy' disks.

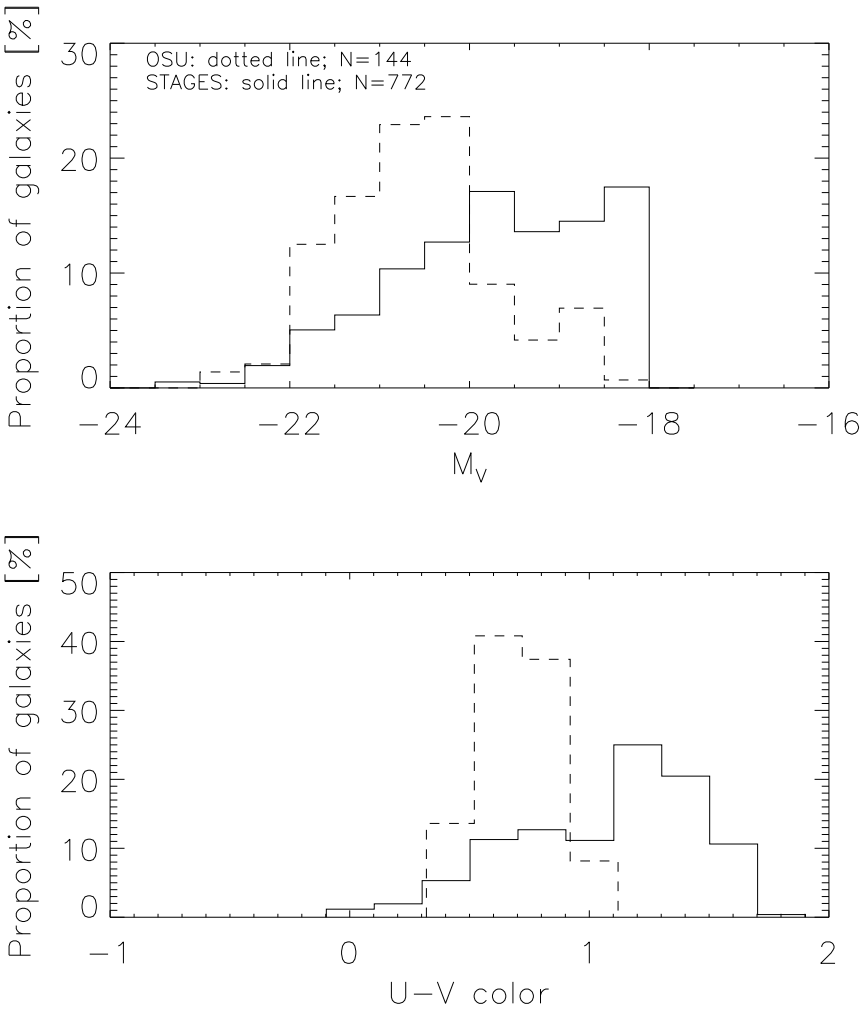

Fig. 16.— The absolute magnitude M_V (a) and rest-frame U-V color (b) distributions are shown for the STAGES (solid line) and OSUBSGS (dotted line). The OSUBSGS sample is both brighter and bluer than the STAGES sample.

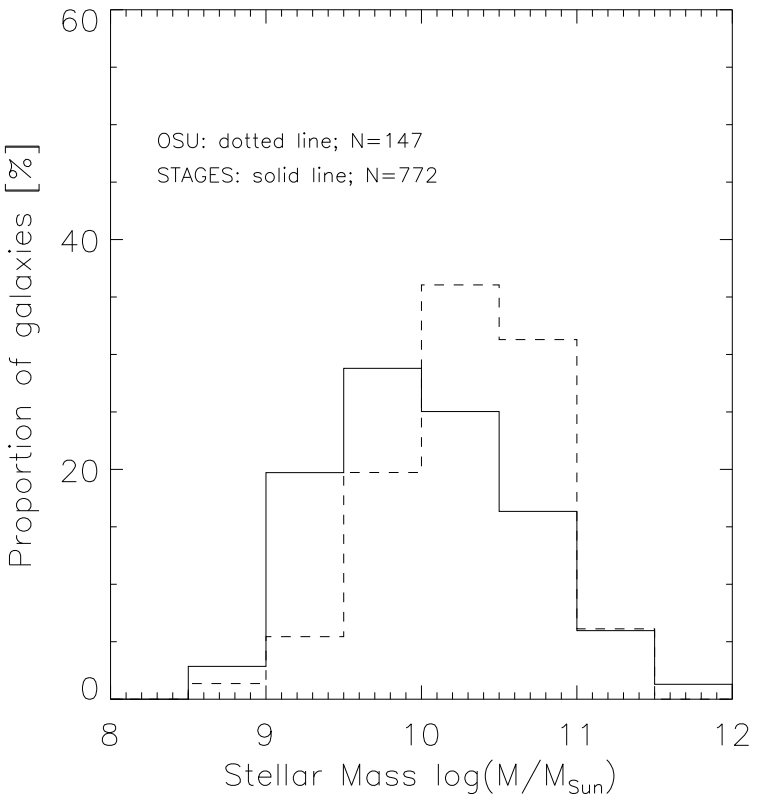

Fig. 17.— The stellar mass distribution of the OSU (dotted line) and STAGES (solid line) samples are overplotted. The two samples have similar range in stellar mass, however, the OSU sample is comprised of slightly more massive galaxies on average.

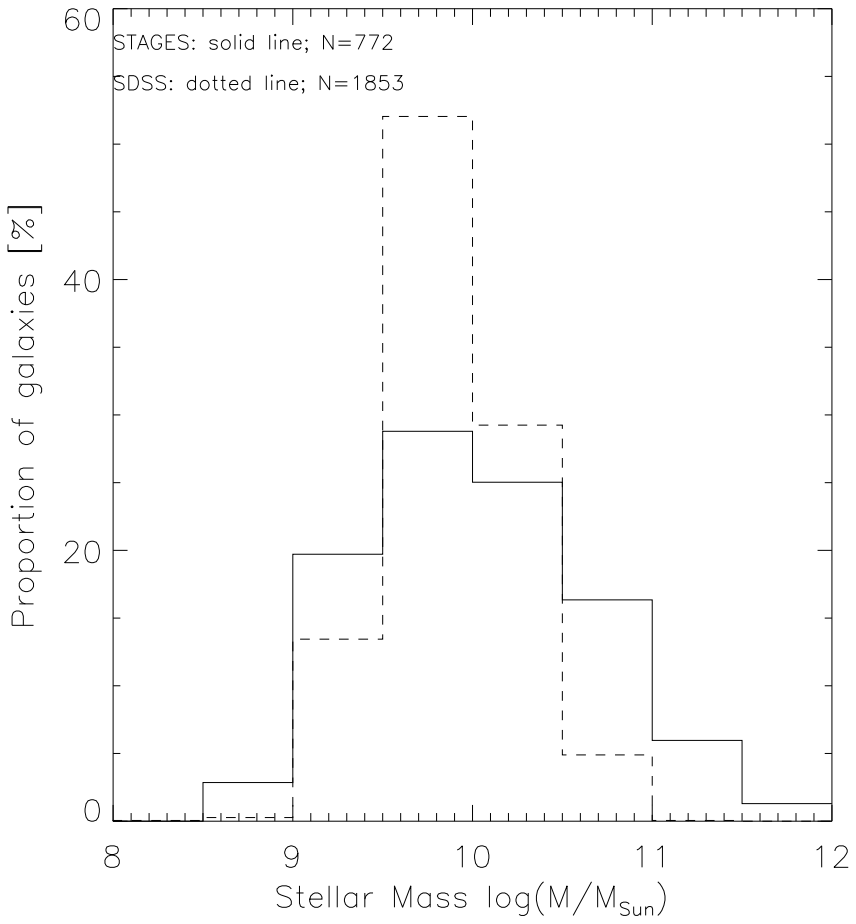

Fig. 18.— The stellar mass distribution of the SDSS (dotted line) and STAGES (solid line) samples are overplotted. The two samples have similar distributions in stellar mass, peaking at $\sim 10^{9.5} M/M_{Sun}$, however the STAGES distribution is wider, and contains galaxies down to 10^8 M/M_{Sun} and up to 10^{12} M/M_{Sun}. SDSS galaxies are found mostly in the range $10^9 - 10^{11}$ M/M_{Sun}.

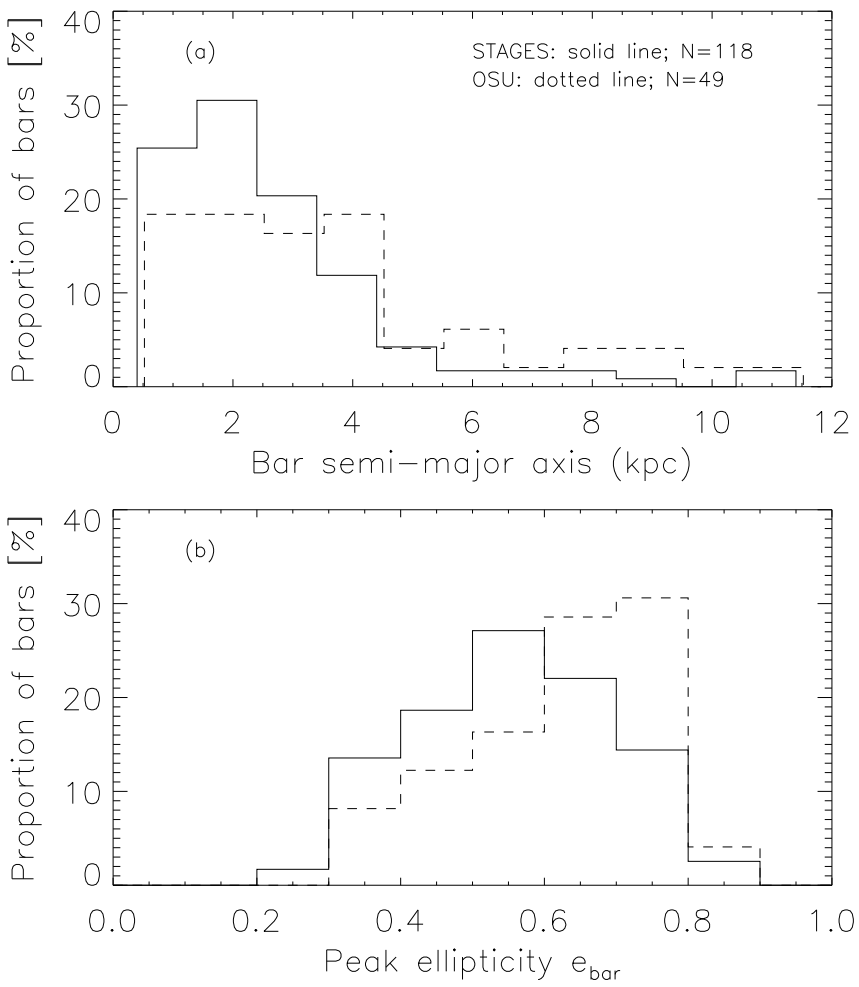

Fig. 19.— (a) Distribution of bar semi-major axis length $a_{\rm bar}$ for the OSUBSGS (dotted line) and STAGES (solid line) samples. The two samples have similar distribution in bar size. (b) Distribution of peak bar ellipticities $e_{\rm bar}$ for the OSUBSGS (dotted line) and STAGES (solid line) samples. Bars in the OSU sample are significantly weighted toward higher ellipticities ($e_{\rm bar} \sim 0.7$) compared to bars in the STAGES sample, whose distribution peaks at $e_{\rm bar} \sim 0.5$.

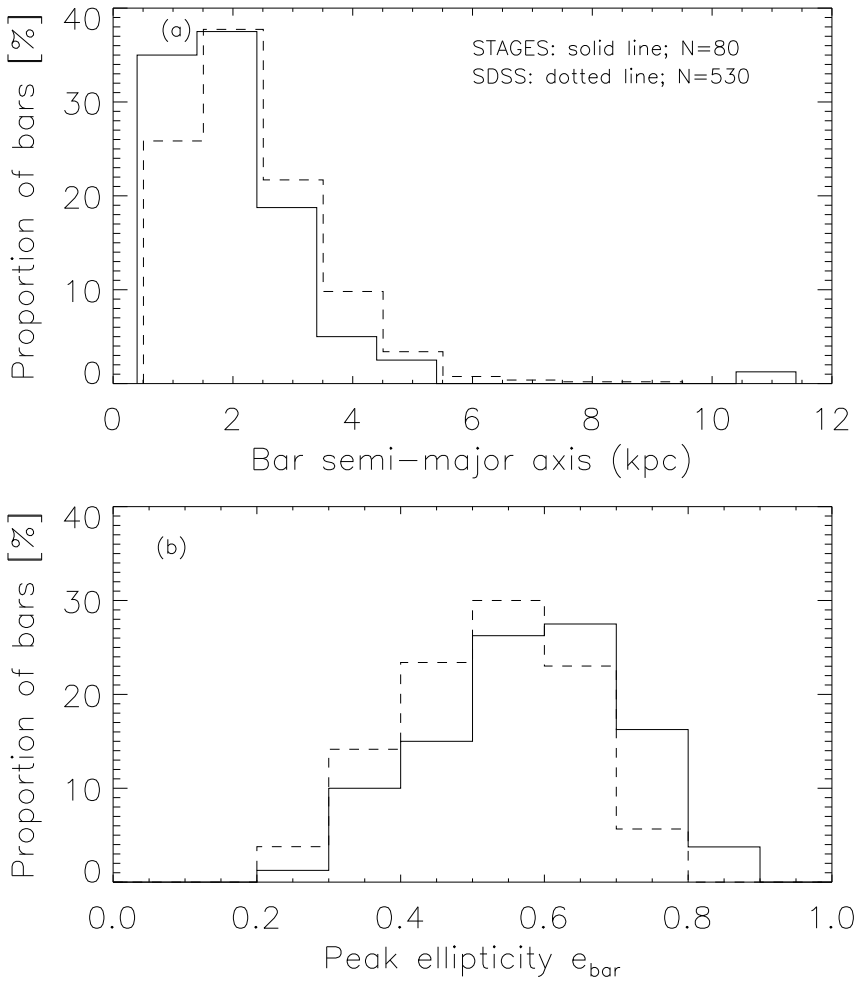

Fig. 20.— (a) Bar semi-major axis distributions $a_{\rm bar}$ for the STAGES (solid line) and SDSS (dotted line) samples. Both samples have similar bar size distributions. (b) Bar peak ellipticity distributions $e_{\rm bar}$ for the STAGES and SDSS distributions. Both samples also have similar ellipticity distributions.